https://doi.org/10.5194/egusphere-2026-3328
Preprint. Discussion started: 3 July 2026

Thermokarst and Microtopography Enhance Carbon Fluxes from an Arctic Tussock Tundra Site

*Kelcy Kent[1], *Kyle A Arndt[1], Danielle Trangmoe[1], Patrick Murphy[1], Sigrid Dengel[3], Margaret Torn[3], Oriana Chafe[3, 4], Marco Montemayor[2], and Susan M. Natali[1]

[1] Woodwell Climate Research Center, Falmouth, MA, 02540, USA
[2] Department of Earth and Planetary Science, University of California Santa Cruz, Santa Cruz, California, 95064, USA
[3] Lawrence Berkeley National Laboratory, Berkeley, CA, 94720, USA
[4] Environmental Studies Program - Department of Biology, University of Oregon, Eugene, OR, 97403, USA

* Authors contributed equally to this work

Correspondence to: Kelcy Kent (kck7bw@virginia.edu)

https://doi.org/10.5194/egusphere-2026-3328
Preprint. Discussion started: 3 July 2026

Abstract

As the Arctic warms, thawing permafrost releases carbon dioxide (CO_2) and methane (CH_4) into the atmosphere, creating a positive feedback to warming. However, carbon loss from permafrost soils is poorly understood due to the paucity of *in-situ* carbon flux measurements from Arctic landscapes, complicating efforts to accurately characterize models. To gain insight into the interannual variability of carbon fluxes in response to environmental conditions, as well as the impact of thermokarst landscape features and microtopography on carbon fluxes, we analyzed a six-year (July 2017 - September 2023) eddy covariance tower (EC) dataset from a tussock tundra site with thermoerosional drainage channels near Council, Alaska. Flux chambers located in upland, lowland, and sloped plots near the EC tower measured differences in carbon fluxes by landscape position and inundation status from 2017 - 2019. EC data indicated Council ranged from a weak net carbon sink (-6.50 g C m^{-2}) to a moderate source (30.93 g C m^{-2}) with higher net carbon emissions during warmer temperatures. Growing season CO_2 uptake was significantly greater from thermokarst drainage channels south of the tower, but CO_2 emissions from these channels were significantly lower in the winter compared to the northern tundra. Similarly, thermokarst, microtopography, and inundation enhanced CH_4 emissions. These findings, which establish a baseline for continued long-term monitoring of carbon fluxes and environmental conditions at the Council tundra site, highlight the importance of including the influence of microtopography and landscape features, such as thermokarst, in assessments of current and future carbon balance of the Arctic.

https://doi.org/10.5194/egusphere-2026-3328
Preprint. Discussion started: 3 July 2026

1. Introduction

Arctic permafrost (ground that remains below 0 ºC for at least two consecutive years) harbors about one third of the global soil carbon pool (Hugelius et al., 2014, 2020; Schuur et al., 2015, 2022), and permafrost regions have historically been an important global carbon sink (Abolt et al., 2020; Hugelius et al., 2014; Schuur et al., 2008, 2015). Accelerated Arctic warming (Rantanen et al., 2022), record-high permafrost temperatures, and permafrost thaw (Biskaborn et al., 2019; Hugelius et al., 2014; Schuur et al., 2022) stand to substantially impact topography, hydrology, vegetation distribution, and infrastructure (Biskaborn et al., 2019; Christiansen et al., 2010; Romanovsky et al., 2010b, a; Smith et al., 2010; Vieira et al., 2010; Zhao et al., 2010). Once thawed, organic-rich material stored in previously frozen permafrost remobilizes and becomes available for microbial decomposition, leading to increased respiration and loss of carbon to the atmosphere in the form of greenhouse gases such as carbon dioxide (CO_2) and methane (CH_4) (Schuur et al., 2015, 2022), acting as a positive feedback mechanism for climate warming.

While gradual permafrost degradation due to warming leads to relatively consistent, incremental changes throughout Arctic landscapes (Luo et al., 2013), ice-rich landscapes can experience abrupt thaw and thermokarst (the process of ground ice degradation, ground subsidence, and often water accumulation) (Webb et al., 2025). Abrupt thaw can be triggered by disturbances (such as fire or changes in vegetation cover) and climate extremes (e.g., uncharacteristically warm or snowy years) (Jorgenson et al., 2022; Kanevskiy et al., 2017; Swanson, 2021; Ward Jones et al., 2019). Around 20% of the northern permafrost region are vulnerable to abrupt thaw and these regions could store approximately half of the region's below-ground organic carbon (Olefeldt et al., 2016). Thermokarst often leads to the formation of pits, troughs, or gullies that impound water or snow, and lead to further erosion and rapid thawing of surrounding permafrost due to soil exposure and increased heat fluxes (Jorgenson et al., 2010; Kokelj and Jorgenson, 2013; Osterkamp et al., 2009). These landscape changes can facilitate the release of large amounts of CH_4 (Walter et al., 2007), a greenhouse gas with 28 times the global warming potential of CO_2 over a 100-year timescale (Forster et al. 2021; (Mar et al., 2022). Abrupt thaw events could emit 60 - 100 GtC by 2300 in addition to the 200 GtC projected from gradual permafrost thawing (Turetsky et al., 2020; Nadeem et al., 2025).This potentially substantial positive permafrost and thermokarst carbon feedback is still poorly understood.

The spatial heterogeneity of Arctic landscapes, and the dynamic microtopography generated by thermokarst, create highly variable spatiotemporal carbon dynamics. Both increased carbon release (Cassidy et al., 2016; Euskirchen et al., 2017) and increased carbon uptake (Lee et al., 2011; Vogel et al., 2009) have been observed from thermokarst features. For example, thermokarst can promote plant productivity and carbon uptake due to an influx of nutrients from thawing soils (Hewitt et al., 2019; Salmon et al., 2016) or increased soil moisture from ground subsidence (Euskirchen et al., 2017; Lee et al., 2011), but can also enhance soil respiration due to deeper thaw and higher soil temperatures (Vogel et al., 2009; Webb et al., 2016). High erosion rates can also redistribute or laterally export carbon out of the system, inhibiting respiration and reducing local carbon emissions (Abbott et al., 2015; Abbott and Jones, 2015). Yet, extensive erosion from thermokarst (Jorgenson and Osterkamp, 2005) and associated ground subsidence

https://doi.org/10.5194/egusphere-2026-3328
Preprint. Discussion started: 3 July 2026

may conversely lead to landscape drying or flooding (Euskirchen et al., 2017), which could disrupt plant growth and diminish carbon uptake as a result of water stress or drowning vegetation.

Thermokarst can also promote higher respiration throughout the cold seasons (fall, winter, and spring) by mediating soil temperature (Vogel et al., 2009; Webb et al., 2016). Thermo-erosional gullies that trap snow can result in deeper snowpacks, which insulate the soils and maintain warmer soil temperatures, thereby benefitting microbial activity and enhancing cold season soil respiration (Lyu and Zhuang, 2018). Studies have shown microbial activity can continue for months after light and temperature limit photosynthetic activity (Jansson and Taş, 2014), and microbial activity and measurable respiration has been recorded down to −39 °C (Panikov et al., 2006), suggesting that microbes can remain active well into the cold season. Data also indicate shoulder season (fall and spring) and winter emissions are significant for both CO_2 (Arndt et al., 2020; Natali et al., 2019; Oechel et al., 2014; Raz-Yaseef et al., 2017) and CH_4 (Arndt et al., 2019, 2020; Zona et al., 2016), and that cold season carbon emissions can be comparable to, or even exceed, growing season carbon uptake (Oechel et al., 2014; Natali et al., 2019). The complexity of thermokarst dynamics pose considerable challenges in incorporating such processes into Earth System Models (Natali et al., 2021; Olefeldt et al., 2016), contributing to the high uncertainty in carbon fluxes and their controls (McGuire et al., 2009; Natali et al., 2021, 2022).

To contribute to a better understanding of interannual patterns in carbon fluxes and budgets from a heterogeneous tundra landscape and how thermokarst may impact carbon fluxes, we analyzed a six-year (2017 – 2022), eddy covariance (EC) record from a tussock tundra site on the Seward Peninsula near Council, Alaska. We investigated patterns in CO_2 and CH_4 fluxes and meteorological variables, and compared interannual and seasonal carbon budgets. We also examined how various landscape features may impact carbon fluxes using both EC data and chamber-based measurements. Council was identified as an important site for improving representativeness of measurements for up-scaling efforts and extrapolating point-measurements to larger landscapes with similar environmental features (Hoffman et al., 2013). The Seward Peninsula is predicted to be representative of what conditions on the North Slope may be by the end of the century (Hoffman et al., 2013). Environmental processes at Council can offer valuable insight into the ecosystem shifts that are likely to occur in northern Alaska due to climate warming, and such data can inform models predicting future trajectories of Arctic tundra carbon dynamics.

2. Methods

2.1 Site Description

The EC tower and soil chamber measurements (Fig. 1) were located in the Seward Peninsula near Council, Alaska (64.8618, -163.7008; Ameriflux site ID: US-NGC). The site is tussock tundra with discontinuous permafrost, further characterized as a wet meadow tundra adjacent to the tundra-forest ecotone (Yang et al. 2021). Low-lying areas with thaw ponds and thaw-pond channels support wet-sedge meadow communities, whereas the surrounding level plain is comprised of tussock tundra vegetation (*Eriophorum vaginatum*) with low shrubs (*Betula nana, Empetrum nigrum,*

https://doi.org/10.5194/egusphere-2026-3328
Preprint. Discussion started: 3 July 2026

Arctostaphylos spp., Rubus chamaemorus, Salix arctica, Salix glauca, Vaccinium spp.), bordered by white spruce (*Picea glauca*) woodlands (Llyod et al. 2003). Additional common species surveyed within the vicinity of the tower in 2025 included *Carex spp*., *Cladonia* lichen, *Andromeda pulchra*, *Rhododendron tomentosum*, and *Sphagnum* and *Polytrichum* moss (Kent et al., 2026).

Mean annual air temperatures from the data collection time period ranged from -4.16 to -0.17 ℃ (Table 1) with a mean of -1.9 ℃ from 2017 – 2022. Multi-year (January 2009 - October 2025) mean monthly rainfall identifies July and August to be the months with the most precipitation (~89 mm and ~112 mm) and April and May to be the months with least precipitation (40.64 mm and 38 mm). Mean monthly snowfall was greatest in February (46.2 cm) and December (38.2 cm) (World Weather Online: https://www.worldweatheronline.com/council-weather-averages/alaska/us.aspx).

2.2 Eddy Covariance Tower Instrumentation

Carbon flux and meteorological data were collected from July 2017 through September 1st, 2023 (Dengel et al., 2020; Dengel and Torn, 2020). The EC tower (2.65 m measurement height; Figs. S1, S2, S3) included an IRGASON integrated CO_2 and H_2O Open-Path Gas Analyzer (with 3-D sonic anemometer) (Campbell Scientific, Logan, UT, USA), and an LI-7700 open-path CH_4 analyzer (LI-COR, Lincoln, NE, USA). Meteorological data were collected with a CNR4 four component radiometer for net radiation (shortwave in and out) (Kipp & Zonen, Delft - The Netherlands), LI-190 quantum sensors for photosynthetically active radiation (LI-COR, Lincoln, NE, USA), an HMP-60 for air temperature and relative humidity (Vaisala Inc., Vantaa, Finland), and HFP-01 ground heat flux plates for ground heat flux (Hukseflux, Delft, The Netherlands). Raw data from the IRGASON, sonic anemometer, and LI-7700 were recorded at 10 Hz on a CR6 datalogger (Campbell Scientific, Logan, UT, USA). Soil moisture content and soil temperature were measured with CS650 30 cm soil water content reflectometers (Campbell Scientific, Logan UT, USA) in four locations near the tower: beneath a tussock, at the edge of a thermokarst pond, at the foot of the EC tower, and in a tundra patch dominated by blueberries and lichens. The CS650 probes were installed at an angle, and measurements were integrated from 0 - 15 cm.

2.3 Chamber Flux Measurements

Measurements were taken from 35 chamber locations placed in various landscape positions near the EC tower (Fig. 1), comprising upland moist acidic tussock tundra (“upland”), thermo-erosional slopes (“slope”), and lowland water channels (“lowland”). All landscape positions, especially lowland positions, were periodically inundated throughout the study period. Data from chamber measurements included CH_4 and CO_2 fluxes, soil temperature, soil moisture, and thaw depth measurements from August 3rd - September 14th, 2016, June 19th - September 10th, 2017, June 21st - August 31st, 2018, and June 20th - 26th, 2019 (see Chafe et al. (2023)). Flux chambers consisted of opaque or transparent closed-loop chambers (25 cm diameter, 15-20 cm height) – tall enough to enclose vegetation – seated on PVC bases extending ~15 cm below the soil surface. To mitigate disturbance, chamber bases were installed at the beginning of the sampling season and left in place throughout the remainder of the season. Chambers were seated in a 3 cm-deep

https://doi.org/10.5194/egusphere-2026-3328
Preprint. Discussion started: 3 July 2026

inundated trench in the base's top rim to ensure an airtight seal and vented according to Xu et al. (2006). Air within the chamber was circulated through the gas analyzer, recording CO_2 and CH_4 concentrations over 4 - 8 minutes. Transparent and opaque chambers were swapped out to record light and dark carbon flux measurements from the same base, allowing for the calculation of net ecosystem exchange (NEE), gross primary productivity (GPP), and ecosystem respiration (R_{eco}) from CO_2 fluxes. The CO_2 flux measurements from transparent (light) chambers represented NEE, measurements from opaque (dark) chambers represented R_{eco}, and GPP was calculated as the difference between light and dark CO_2 flux measurements. Chamber flux measurements were measured with either a Los Gatos Research, Inc. (LGR) Ultraportable Greenhouse Gas Analyzer or a Picarro G4301 Mobile Gas Concentration Analyzer. Both instruments use Cavity Ring-Down Spectroscopy to analyze CO_2 and CH_4 concentrations, and measurements from both gas chambers were compared for July 18, 2018 to confirm instrument agreement (Chafe et al., 2023).

Soil volumetric water content was calculated using the internal calibration of a MiniTrase TDR (Soilmoisture Equipment Corp., Goleta, CA, USA) and integrated over the top 20 cm of the soil profile. Soil temperature was measured with a thermocouple probe at 10 and 20 cm below the ground surface. As vegetation and inundation varied among plots, the depths of moisture and temperature measurements were taken from the top of the moss layer or bare soil. Thaw depth was determined by manually inserting an 80-cm long metal tile probe into the soil and measuring the depth of insertion from the top of the moss layer to the top of the permafrost table. Periodic measurements were taken from August 2016 through June 2019 (Chafe et al., 2023). Out of 216 measurements, 30 were deeper than the length of the thaw probe.

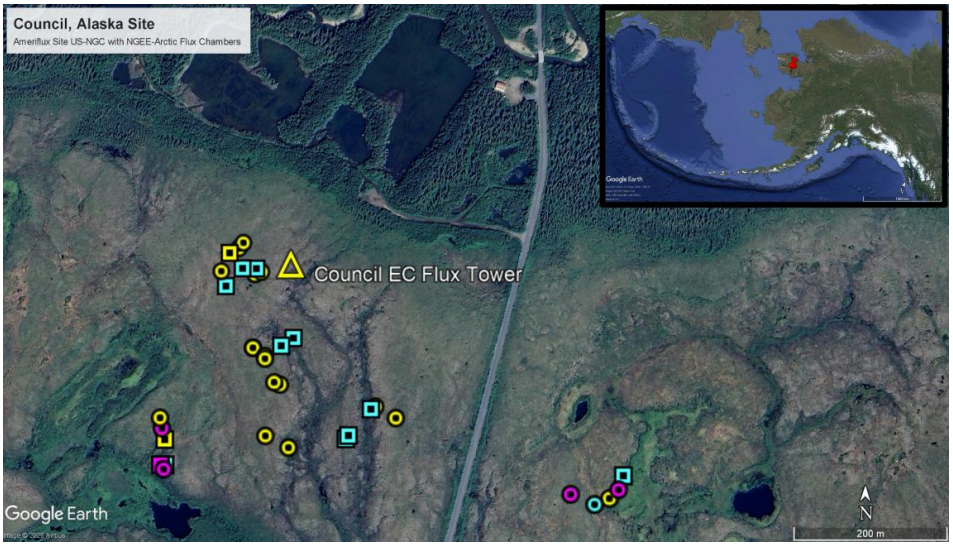

Figure 1. Location of the eddy covariance (EC) tower site (yellow triangle; Ameriflux: US-NGC) with the locations of the soil chambers. Yellow points represent upland plots, purple points represent slope plots, and blue points represent lowland plots; square shapes indicate plots that were periodically inundated during the study period. (Imagery © 2026 Airbus, Map data © 2025 Google Earth; Inset map: Imagery © Landsat / Copernicus and IBCAO, Data © SIO, NOAA, U.S. Navy, NGA, GEBOO, LDEO-Columbia, NSF)

https://doi.org/10.5194/egusphere-2026-3328
Preprint. Discussion started: 3 July 2026

2.4 Eddy Covariance Data Processing

The high-frequency (10 Hz) flux data were processed with EddyPro® (Version 6.2.1; LI-COR®) to provide half-hourly fluxes detailed in Dengel et al. (in review). Standard corrections, including frequency corrections (Massman, 2000), were applied with the Webb-Pearman-Leuning correction (Webb et al., 1980), and spectroscopic corrections were applied to the LI-7700 CH_4 analyzer (McDermitt et al., 2011). Data were not gap-filled, and were quality controlled by removing outliers beyond feasible limits, rain events (Burba, 2013), and by following Foken at al. (2004). For additional cleaning, we fit an autoregressive integrated moving average (ARIMA) model to time-series data to calculate a one week rolling median average deviation. For energy and CO_2 fluxes, all measurements three median average deviations away from the ARIMA model were removed while eight median average deviations were used for CH_4 given the greater stochasticity of CH_4 emissions. Meteorological data were collected at lower frequencies and recorded as half-hourly averages.

2.5 Calculating Carbon Budgets

To calculate total carbon budgets, flux data were gap-filled using a random forest model (randomForest v4.7-1.2; Liaw and Wiener 2022) trained with the following meteorological variables: soil temperature, soil moisture, global radiation, relative humidity, wind speed, wind direction, vapor pressure deficit, latent heat flux, and sensible heat flux. To ensure complete, comprehensive datasets for model training, these meteorological data were taken from the global climate reanalysis dataset ERA5 (C3S, 2018). To better fit site conditions, the ERA5 dataset was modified based on site measurements via a linear regression (Fig. S4). Due to the poor agreement between ERA5 soil moisture variables and measured soil moisture at the site, a random forest model was also used to gap-fill missing soil moisture measurements for model training (Figs. S4 & S5). The optimum number of trees used in the random forest models was determined with model out-of-bag (OOB) error. Iterations of the models were run using ntree = 50 to ntree = 1000, increasing trees by 100 for each iteration. The optimum model was recognized as the model with the lowest number of trees where subsequent iterations did not markedly improve. Then, separate models were run for gap-filling CO_2 (ntree = 850) and CH_4 fluxes (ntree = 950) using the half-hourly measured fluxes across all years (July 16, 2017 - August 31, 2023). Fluxes were partitioned with the "ReddyProc" package in R (Wutzler et al., 2018); gross primary productivity (GPP) and ecosystem respiration (R_{ECO}) were estimated following a nighttime partitioning method (Reichstein et al., 2005). Calculated CO_2 and CH_4 budgets represent carbon-equivalent budgets.

2.6 Seasonal Delineations and Budgets

Each year was divided into three seasons: winter, growing season, and fall senescence. Seasons were based on air temperature and whether NEE (net CO_2 flux) was positive (CO_2 release) or negative (CO_2 uptake). As site-modified ERA5 air and soil temperatures agreed well (Figs. S4 & S6) with measured air (slope = 0.94, R^2 = 0.96) and soil temperature (slope = 0.80, R^2 = 0.87), site-modified ERA5 values were used to gap-fill missing air and soil temperature measurements to allow more representative seasonal delineations and seasonal and annual means.

https://doi.org/10.5194/egusphere-2026-3328
Preprint. Discussion started: 3 July 2026

The growing season start was identified as the first of four consecutive days of negative mean daily NEE (indicating uptake and a net CO_2 sink) and ended on the first of four consecutive days of positive mean daily NEE (indicating net CO_2 release). The start of winter was defined as the first of four consecutive days of gap-filled air temperature at or below 0 °C. To allow for continuous winter seasons, the winter of each year spanned into the following year, ending the day before the start of the next growing season (i.e., winter of 2022 spanned late 2022 to early 2023; calendar year fluxes can be found in Table S1). The interim between the end of growing season and start of winter, where mean daily NEE was net positive before air temperatures reached freezing, was classified as the fall senescence period. Growing season and fall carbon budgets were calculated for each year as the sum of daily mean carbon fluxes for that season. Annual carbon budgets were calculated as the sum of seasonal budgets, including the continuous winter. Annual means and standard error of meteorological variables were calculated based on calendar year (Table 1); additional calendar year carbon budget calculations and meteorological variable means can be found in the supplemental material (Table S1). The EC tower record ended on September 1st, 2023. Since 2023 was therefore incomplete and seasonal delineations beyond the end of the 2022 - 2023 winter season could not be identified, 2023 was excluded from interannual variability assessments, budgets, and seasonal comparisons.

2.6.1 Winter Carbon Budget Calculations

Most years had little to no winter CO_2 or CH_4 flux measurements (data coverage ranging from 1.3 to ~31% for CO_2 and 0 to ~39% for CH_4; Fig. 2 & Table S2), resulting in insufficient winter data to adequately train a random forest model for gap-filling. While models evaluating temperature-flux relationships performed well, these models did not perform well when soil temperatures were below 0 °C nor did a linear or exponential temperature model derived from 2018 - 2019 winter measurements (the winter with the best data coverage) (Fig. S7). Therefore, as the winter of 2018 - 2019 had the best winter CO_2 and CH_4 measurement coverage (31.1% and 38.8%, respectively), we used that winter year to determine a proportional winter CO_2 and CH_4 budget adjustment to apply to the other years. We calculated the proportion of daily mean winter CH_4 fluxes to daily mean growing season CH_4 fluxes based on measurements from 2018, and found that daily mean winter CH_4 fluxes amounted to ~44% of the daily mean growing season flux. For each year, the daily mean winter CH_4 flux was calculated as ~44% of that year's daily mean growing season CH_4 flux. The mean daily winter flux was then multiplied by the number of days within each year's respective winter season to obtain a seasonal winter budget. Likewise, we found that the daily mean winter CO_2 flux amounted to ~45% of the daily mean growing season flux, and winter CO_2 budgets were calculated for other years using the same method.

2.7 Statistical Analyses

Daily means of carbon fluxes used in statistical analyses were calculated from half-hourly measurements using a 50% data-availability threshold to ensure good representation. To capture short nighttime periods and because nighttime conditions and fluxes are more stable, the threshold for daily mean nighttime CO_2 flux calculations was lowered to 10%. Nighttime CO_2 fluxes were identified as fluxes measured when incoming shortwave radiation was less than or equal to 20 W m^{-2}. As the dominant landscape type within the EC footprint (Fig. 1; Figs. S2, S3) was tussock tundra, we used the tussock probe for statistical analysis that included soil temperature and soil moisture. Additionally, soil

https://doi.org/10.5194/egusphere-2026-3328
Preprint. Discussion started: 3 July 2026

moisture measurements were constrained to time periods when soil temperature was above 2 °C to avoid potential probe freeze-thaw interference as described by Salmabadi et al. (2025). All statistical analyses were performed in R v4.4.2 (R Core Team, 2024).

2.7.1 Eddy Covariance Tower Measurements

Time Series Analyses

Patterns in seasonal and annual means of NEE, CH_4 flux, and total carbon budgets (the sum of NEE and CH_4 budgets), gap-filled soil and air temperature, vapor pressure deficit, soil moisture from unfrozen ground, relative humidity, sensible heat, latent heat, and ground heat flux across years were assessed with Mann-Kendall trend tests (package: "Kendall", McLeod 2022).

Variable Importance for NEE and CH_4

Variable importance for CO_2 and CH_4 flux was determined using a random forest algorithm (randomForest v4.7-1.2 package in R; Liaw and Wiener, 2022) and the percent increase in mean squared error (%IncMSE), which determines the %IncMSE (i.e., decrease in model accuracy) when a variable is removed from the model. Separate models were run for NEE (ntree = 850) and CH_4 flux (ntree = 950) using the half-hourly measured carbon flux and meteorological data from all years (2017 - 2023). Model variables included were wind direction, soil moisture, soil temperature, air temperature, shortwave-in, relative humidity, wind speed, latent heat flux, sensible heat flux, ground heat flux, vapor pressure deficit, and a soil temperature-soil moisture interaction term. To address collinear predictors, we used a stepwise approach of reduced models to isolate the most influential variables (Figs. S8 & S9). Variables were removed based on model variable inflation factor (VIF) values and %IncMSE. Starting with the full model, first the soil moisture - soil temperature interaction term was removed, and then the variable with the highest VIF value was removed in subsequent models until all VIF values were below a value of 2. For both CO_2 and CH_4, measured soil moisture (all measurements), wind direction, sensible heat flux, wind speed, ground heat flux, and relative humidity were included in the final models.

Carbon and Meteorological Variable Regressions

Daily means of measured half-hourly CO_2 and CH_4 fluxes were regressed against daily means of meteorological variables using generalized least squares (GLS) models with first-order autoregressive (AR(1)) correlation structures to resolve autocorrelation. Meteorological variables consisted of gap-filled soil and air temperature, vapor pressure deficit, soil moisture, relative humidity, sensible heat flux, latent heat flux, and ground heat flux. Daily mean regressions were restricted to the growing season to avoid potential skews resulting from a paucity of cold season data. Seasonal and annual carbon budgets (CO_2 budget, CH_4 budget, total carbon budget) for each year were also regressed against annual and seasonal means of meteorological variables using Kendall's tau rank correlation tests to account for the small sample size (n = 6) (package: "Kendall", McLeod 2025).

https://doi.org/10.5194/egusphere-2026-3328
Preprint. Discussion started: 3 July 2026

To assess temperature sensitivity, daily means of half-hourly measured nighttime CO_2 fluxes and measured soil temperature relationships were evaluated by generalized nonlinear least squares (GNLS) models with (AR(1)) correlation structures. The nighttime CO_2 - temperature relationship was tested on data from all seasons. Soil temperatures below 0 °C exhibited a spike in CH_4, generating a quadratic U-shaped trendline likely not due to biological conditions (Fig. S10); the CH_4 - temperature relationship therefore excluded the winter. Additionally, using gap-filled air temperature, growing degree days (GDD) and number of GDDs were calculated for each year for time series analyses. Annual GDDs as well as growing season GDD were regressed against CO_2, CH_4, and total carbon budgets with Kendall's tau tests (package: "cor.test" with method = "kendall"). GDDs were calculated with a base temperature of 0 °C (Elmendorf and Hollister, 2023; Tieszen, 1978).

Landscape Feature Partitioning by Wind Direction

We evaluated daily mean carbon fluxes by wind direction to evaluate differences based on the tower footprint. The Council tower site features tundra bordering riparian areas and ponds to the north (N, NE, NW), wet lowlands to the west (W, SW), open tundra to the east (E), and thermokarst / drainage channels to the south (S, SE) (Fig. 1 & Fig. S3). To align wind direction with daily means of carbon fluxes, we assigned a prevailing wind direction to each day based on wind direction frequency counts from the half-hourly measurements taken that day. Prevailing wind directions were binned by landscape features (as described above) to explore whether these landscape features impacted carbon fluxes. Differences in seasonal CO_2 and CH_4 fluxes by wind direction and landscape features were assessed with Kruskal-Wallis tests and post-hoc Dunn tests with Benjamini-Hochberg corrections. Only wind directions and landscape features with at least five daily means (n = 5) were used in statistical analyses.

2.7.2 Flux Chambers

Differences in environmental characteristics (air temperature, soil temperature, thaw depth, soil moisture) and carbon fluxes from the various landscape positions (upland, lowland, slope) were evaluated with Kruskal-Wallis tests. Post-hoc Dunn tests with Benjamini-Hochberg corrections were used to identify statistically significant groupings among landscape positions. Differences in carbon fluxes from inundated or not inundated landscape positions were assessed with Wilcoxon rank sum tests. Due to a low number of observations (n = 2), inundated slope plot measurements were excluded from analyses. An additional measurement (from plot BG 15 on June 20th, 2019) where the reported CH_4 flux was more than double the next highest data-point was removed as an outlier to mitigate skew in calculating means.

3. Results

3.1 Meteorological Patterns

Mean air and soil temperature, and soil moisture, varied by year, with warmer and wetter conditions recorded in 2018-2019 and 2019-2020 followed by relatively cooler and drier conditions in following years (Table 1). Yet, there were no detected annual or seasonal trends in gap-filled air and soil temperature, soil moisture (unfrozen), sensible heat flux, latent heat flux, ground heat flux, GDD, and number of GDD across the six years of measurements. However,

https://doi.org/10.5194/egusphere-2026-3328
Preprint. Discussion started: 3 July 2026

there was a significant (p = 0.01) decrease in mean annual relatively humidity (tau = -1.0, sens slope = -6.32) and a significant (p = 0.02) increase in mean annual vapor pressure deficit (tau = 0.87, sens slope = 0.89) across years (Fig. S13). Likewise, seasonal Mann-Kendall time series analyses found a significant trend in decreasing relative humidity (p = 0.01) each season, with a significant trend in increasing vapor pressure deficit (VPD) (p = 0.02) during the growing season and fall senescence (Figs. S14 & S15; Table S3).

3.2 Carbon Budgets

3.2.1 Annual Carbon Budgets

Annual CO_2 budgets were typically a net source of 7.15 ± 5.22 g CO_2-C m^{-2} y^{-1} ranging from a sink of -8.43 g CO_2-C m^{-2} to a source of 27.17 g CO_2-C m^{-2} (Table 1; Fig. 3). Annual CH_4 budgets were always a net source ranging from 1.44 to 3.75 g CH_4-C m^{-2}. Overall, the Council site was a net carbon source during the study period, with a mean annual budget of 7.15 ± 5.22 g CO_2-C m^{-2} y^{-1} and 2.41 ± 0.31 g CH_4-C m^{-2} y^{-1}, amounting to 9.57 ± 5.42 g C m^{-2} y^{-1} in mean net annual carbon emissions (Table 1; Fig. 3). Only 2017 - 2018 was a net annual carbon sink (-6.50 g C m^{-2}) with the remaining years ranging from 1.61 to 30.93 g C m^{-2}. Cumulatively, Council produced 42.93 g CO_2-C m^{-2} in CO_2 emissions and 14.48 g CH_4-C m^{-2} in CH_4 emissions, leading to total net carbon emissions of 57.40 g C m^{-2} from the site over the course of the six-year study period (Table 1; Fig. 3). Mann-Kendall time series tests found no significant trends in mean annual CO_2, CH_4, or total net carbon budgets across years.

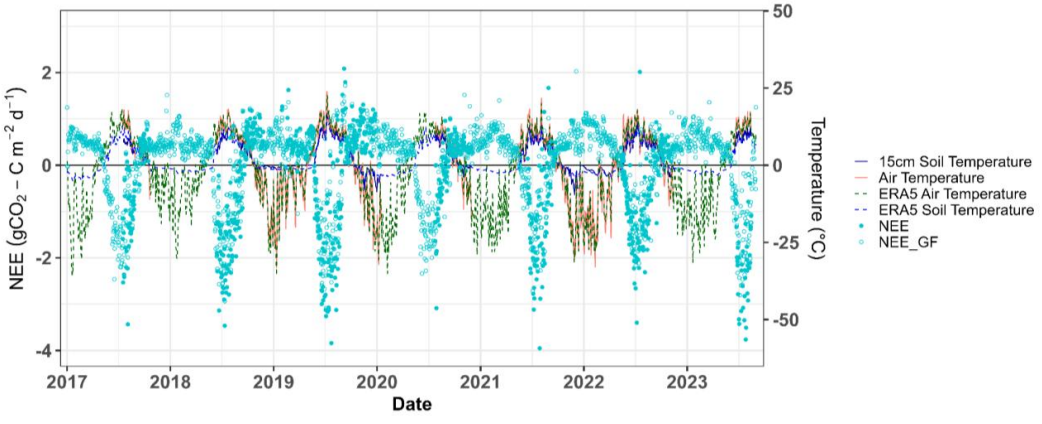

Figure 2. Trends of measured daily mean net ecosystem exchange (NEE), gap-filled daily mean NEE (NEE_GF), site air temperature , ERA5 air temperature, site soil temperature, and ERA5 soil temperature (7 – 20 cm) for the Council, Alaska site (AMF ID: US-NGC) from January 2017 to September 2023.

3.2.2 Seasonal Carbon Budgets

Following typical seasonal patterns of Arctic tundra, the Council site was a net carbon sink during the growing season and a net carbon source during fall senescence and winter seasons (Table 1; Fig. 3). Seasonal carbon budgets suggested

https://doi.org/10.5194/egusphere-2026-3328
Preprint. Discussion started: 3 July 2026

weakening growing season CO_2 sinks (less CO_2 uptake) over the course of the study (Fig. 3; Fig. S16). Fall and winter season CO_2 emissions increased in the first three years of the study then declined to lower emissions levels in the latter three years (Table 1; Fig. 3; Fig. S16). Similarly, CH_4 emissions peaked in 2019 and declined in following years across all seasons. Net carbon budgets mirrored patterns in CO_2 budgets, where earlier years were slightly stronger total carbon sinks compared to the latter three years (Fig. 3).

Table 1. Mean (± SE) daily net ecosystem exchange (NEE) and methane (CH_4) flux by season, seasonal and winter-year annual net CO_2, CH_4, and total carbon budgets (g C/m^2), and mean seasonal and annual gap-filled air and soil temperature, soil moisture, and number of days within season across years. Calendar-year annual means for air and soil temperature also reported. The " * " notation by winter fluxes and budgets reflect winter CO_2 and CH_4 emissions that were calculated as a proportion of the daily average growing season flux – as determined by the measurements from 2018 – multiplied by the number of days within each year's respective winter season. (Percent gap-filled can be found in Table S2; calendar-year fluxes, carbon budgets, and meteorological means can be found in Table S1.)

Year	Season	Adjusted Daily NEE (μmol CO_2 m^{-2} s^{-1})	Adjusted Daily CH_4 Flux (nmol CH_4 m^{-2} s^{-1})	Adjusted Net CO_2 Budget (gC m^{-2})	Adjusted Net CH_4 Budget (gC m^{-2})	Total Net C Budget (gC m^{-2})	ERA5-Gapfilled Air Temperature (°C)	ERA5-Gapfilled Soil Temperature (°C)	SWC (%)	Season Length (days)
2017	Growing Season	-0.88 ± 0.06	7.83 ± 0.25	-116.17	1.03	-115.14	10.29 ± 0.36	6.33 ± 2.82	59.79 ± 0.17	127
	Fall Senescence	0.44 ± 0.04	2.82 ± 0.23	14.5	0.09	14.59	3.85 ± 0.38	2.30 ± 0.90	60.11 ± 0.09	32
	Winter of 2017 - 2018 *	0.40 ± 0.03 *	3.47 ± 0.11 *	93.24	0.81	94.05	-6.66 ± 0.50	-1.43 ± 0.58	-	226
	Annual Mean	-	-	-	-	-	-1.58 ± 0.63	1.07 ± 4.53	-	365
	2017 - 2018 Carbon Budget	-	-	**-8.43**	**1.93**	**-6.50**	-	-	-	-
2018	Growing Season	-1.02 ± 0.07	9.77 ± 0.37	-112.11	1.07	-111.04	11.32 ± 0.28	7.56 ± 2.44	55.68 ± 0.95	106
	Fall Senescence	0.60 ± 0.04	9.61 ± 0.48	26.83	0.43	27.26	5.46 ± 0.52	3.66 ± 2.43	66.01 ± 0.31	43
	Winter of 2018 - 2019*	0.46 ± 0.03 *	4.33 ± 0.16 *	99.70	0.94	100.63	-7.06 ± 0.57	-0.32 ± 0.46	-	209
	Annual Mean	-	-	-	-	-	-0.62 ± 0.58	1.83 ± 4.32	-	365
	2018 - 2019 Carbon Budget	-	-	**14.42**	**2.44**	**16.85**	-	-	-	-
2019	Growing Season	-1.12 ± 0.09	15.22 ± 0.65	-114.86	1.56	-113.29	12.64 ± 0.35	9.77 ± 3.29	56.98 ± 1.10	99
	Fall Senescence	0.68 ± 0.06	15.98 ± 0.64	29.01	0.68	29.69	6.67 ± 0.66	5.24 ± 3.35	67.33 ± 0.51	41
	Winter of 2019 - 2020 *	0.50 ± 0.04 *	6.74 ± 0.29 *	113.02	1.51	114.53	-11.04 ± 0.68	-2.65 ± 1.52	-	216
	Annual Mean	-	-	-	-	-	-0.17 ± 0.59	2.64 ± 5.32	-	365
	2019 - 2020 Carbon Budget	-	-	**27.17**	**3.75**	**30.93**	-	-	-	-
2020	Growing Season	-0.86 ± 0.06	9.33 ± 0.27	-101.86	1.1	-100.76	10.90 ± 0.26	7.70 ± 2.39	58.72 ± 0.19	114
	Fall Senescence	0.35 ± 0.04	7.80 ± 0.46	18.46	0.41	18.87	3.50 ± 0.48	2.45 ± 2.53	60.10 ± 0.52	51
	Winter of 2020 - 2021 *	0.39 ± 0.03 *	4.13 ± 0.12 *	83.82	0.89	84.71	-10.92 ± 0.62	-1.47 ± 0.83	-	208
	Annual Mean	-	-	-	-	-	-2.43 ± 0.66	1.51 ± 4.84	-	365
	2020 - 2021 Carbon Budget	-	-	**0.42**	**2.40**	**2.82**	-	-	-	-
2021	Growing Season	-0.77 ± 0.07	10.53 ± 0.37	-89.89	1.23	-88.66	9.93 ± 0.36	7.38 ± 2.59	53.50 ± 1.40	113
	Fall Senescence	0.28 ± 0.03	6.79 ± 0.43	7.91	0.19	8.1	1.87 ± 0.61	1.41 ± 2.38	60.67 ± 0.48	27
	Winter of 2021 - 2022 *	0.35 ± 0.03 *	4.66 ± 0.17 *	81.08	1.09	82.17	-11.13 ± 0.67	-1.82 ± 2.03	-	226
	Annual Mean	-	-	-	-	-	-4.16 ± 0.67	1.16 ± 4.73	-	365
	2021 - 2022 Carbon Budget	-	-	**-0.90**	**2.51**	**1.61**	-	-	-	-
2022	Growing Season	-0.82 ± 0.06	5.52 ± 0.27	-91.43	0.61	-90.82	10.65 ± 0.32	8.14 ± 2.38	47.42 ± 1.12	107
	Fall Senescence	0.27 ± 0.06	6.74 ± 0.53	8.81	0.22	9.02	5.72 ± 0.46	4.37 ± 2.34	59.71 ± 0.45	31
	Winter of 2022 - 2023 *	0.37 ± 0.03 *	2.44 ± 0.12 *	92.88	0.61	93.49	-9.53 ± 0.58	-1.81 ± 0.81	-	241
	Annual Mean	-	-	-	-	-	-2.22 ± 0.63	1.91 ± 4.68	-	365
	2022 - 2023 Carbon Budget	-	-	**10.26**	**1.44**	**11.69**	-	-	-	-

https://doi.org/10.5194/egusphere-2026-3328
Preprint. Discussion started: 3 July 2026

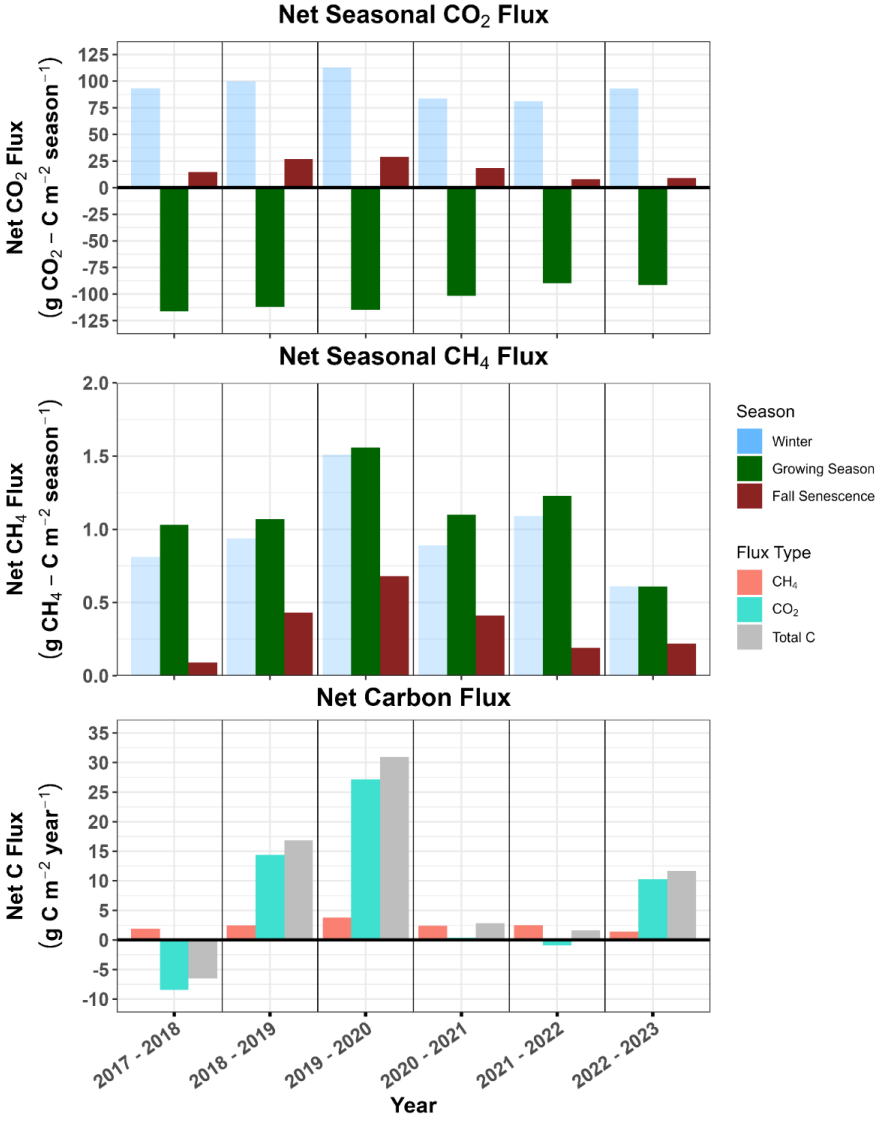

Figure 3. Net seasonal and annual carbon dioxide (CO_2) and methane (CH_4) budgets for 2017 – 2022 from the eddy covariance tower.

3.3 Meteorological Drivers of Carbon Fluxes

The random forest regression analysis showed the most important meteorological variables for NEE were sensible heat flux (380 %IncMSE), soil moisture (179 %IncMSE), and relative humidity (124 %IncMSE) (Fig. S17), whereas

https://doi.org/10.5194/egusphere-2026-3328
Preprint. Discussion started: 3 July 2026

the most important variables for CH_4 were soil moisture (184 %IncMSE), wind direction (181 %IncMSE), and sensible heat flux (137 %IncMSE).

Seasonal and annual means of gap-filled air and soil temperature, soil moisture, vapor pressure deficit, relative humidity, sensible heat flux, latent heat flux, and ground heat flux were regressed against seasonal mean NEE and CH_4 fluxes, as well as seasonal and annual CO_2, CH_4, and total carbon budgets. Per Kendall's tau tests, no significant correlations were found among annual or seasonal means of most meteorological variables and carbon fluxes (CO_2, CH_4, total C), except for a marginally significant and positive relationship between growing season relative humidity and CO_2 and total carbon (tau = -0.73; p = 0.056 for both) (Fig. S18). While annual CO_2, CH_4, and total carbon budgets were not significantly related to annual GDD, there was a significant correlation between greater growing season CO_2 and total C uptake budgets and GDD (tau = -0.87, p = 0.02 for both; Fig. S19).

Growing season daily mean half-hourly CO_2 and CH_4 fluxes regressed against daily means of meteorological variables yielded significant, but weak correlations. Weak, slightly negative correlations existed between CO_2 fluxes and gap-filled air temperature (R^2 = 0.06, slope = -0.04, p = 0.02), gap-filled soil temperature (R^2 = 0.09, slope = -0.09, p <0.001), latent heat flux (R^2 = 0.29, slope = -0.03, p<0.001), sensible heat flux (R^2 = 0.19, slope = -0.02, p<0.001), and soil heat flux (R^2 = 0.06, slope = -0.01, p<0.001). Weak, slightly positive correlations were found between CH_4 and soil moisture (R^2 = 0.14, slope = 0.12, p = 0.01), relative humidity (R^2 = 0.11, slope = 0.1, p<0.001), and sensible heat (R^2 = 0.01, slope = 0.02, p = 0.02), and there were weak, slightly negative correlations with VPD (R^2 = 0.04, slope = -0.24, p = 0.02) and soil heat flux (R^2 = 0.05, slope = -0.05, p = 0.002) (Figs. S20 and S21).

Daily means of half-hourly nighttime CO_2 fluxes exhibited a significant exponential relationship with measured (not gap-filled) soil temperature (R^2 = 0.35, p < 0.001; Fig. 4). The relationship between soil temperature and daily averages of half-hourly CH_4 fluxes, however, resembled a U-shape, indicating a non-monotonic relationship (Fig. S10). The relationship was weak (R^2 = 0.16) but significant (p<0.001). When soil temperatures from the winter season were removed, there was a weak but significant exponential relationship (R^2 = 0.077, p = 0.024) (Fig. 4).

https://doi.org/10.5194/egusphere-2026-3328
Preprint. Discussion started: 3 July 2026

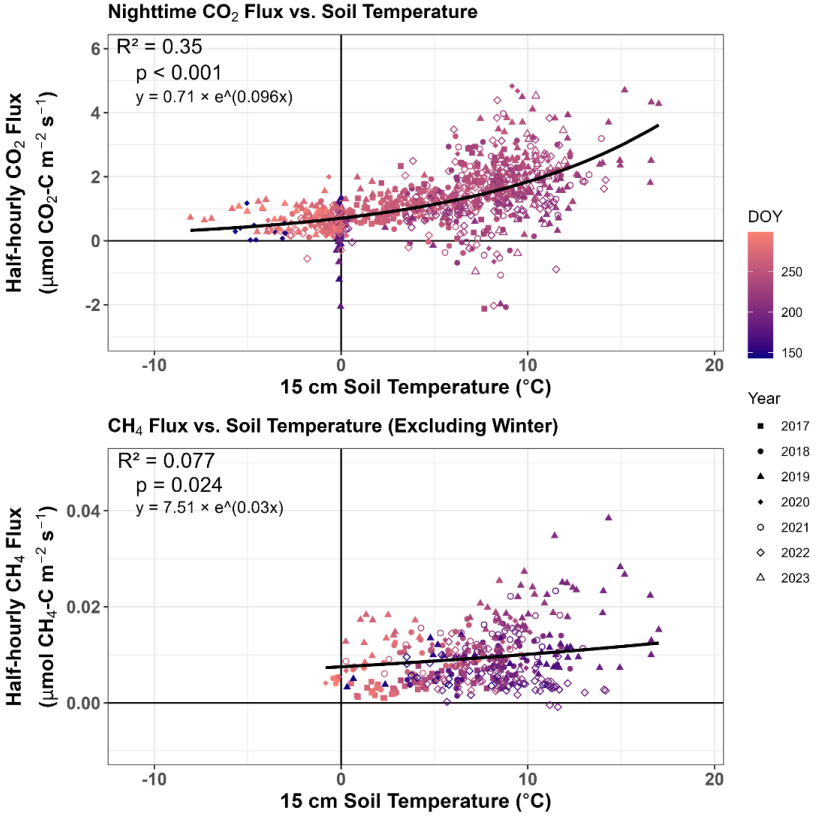

411

412 **Figure 4. Daily averages of half-hourly nighttime CO_2 fluxes (top) and CH_4 fluxes excluding winter (bottom) plotted against**
413 **measured soil temperature integrated over 0 - 15 cm. Different colors represent different days of the year (DOY), and**
414 **different shapes represent different years (2017 – 2023).**

415

416 **3.3 Impact of Landscape Features on Carbon Fluxes**

417 Notable differences in mean seasonal CO_2 and CH_4 fluxes by wind direction were observed. There were significant
418 differences in growing season mean CO_2 and CH_4 fluxes by wind direction ($p = 0.006$ and $p < 0.001$, respectively;
419 Figs. S23 & S24) as well as significant differences in winter CO_2 fluxes ($p < 0.001$) (Fig. S24). Wind directions binned
420 by landscape features (Fig. 5) identified significantly lower growing season ($p<0.001$) CO_2 uptake when winds came
421 from the tundra bordering the forested riparian areas to the north (-1.08 ± 0.05 µmol CO_2 m^{-2} s^{-1}) compared to when
422 wind came from the thermokarst drainage channels to the south (-1.41 ± 0.09 µmol CO_2 m^{-2} s^{-1}). Similarly, winter CO_2
423 emissions were significantly greater ($p = 0.01$) when wind came from the tundra bordering the forested riparian area
424 to the north (0.55 ± 0.02 µmol CO_2 m^{-2} s^{-1}) compared to thermokarst drainage channels in the south (0.33 ± 0.10 µmol
425 CO_2 m^{-2} s^{-1}). Conversely, mean growing season CH_4 fluxes were significantly greater when winds came from the

https://doi.org/10.5194/egusphere-2026-3328
Preprint. Discussion started: 3 July 2026

southern thermokarst drainage channels (0.01 ± 0.0007 µmol CH_4 m^{-2} s^{-1}) compared to fluxes when wind came from the northern tundra bordering the forested riparian area (0.008 ± 0.0003 µmol CH_4-C m^{-2} s^{-1}; $p < 0.001$) and tundra, wet lowland areas to the west and south-west (0.01 ± 0.001 µmol CH_4 m^{-2} s^{-1}; $p = 0.02$).

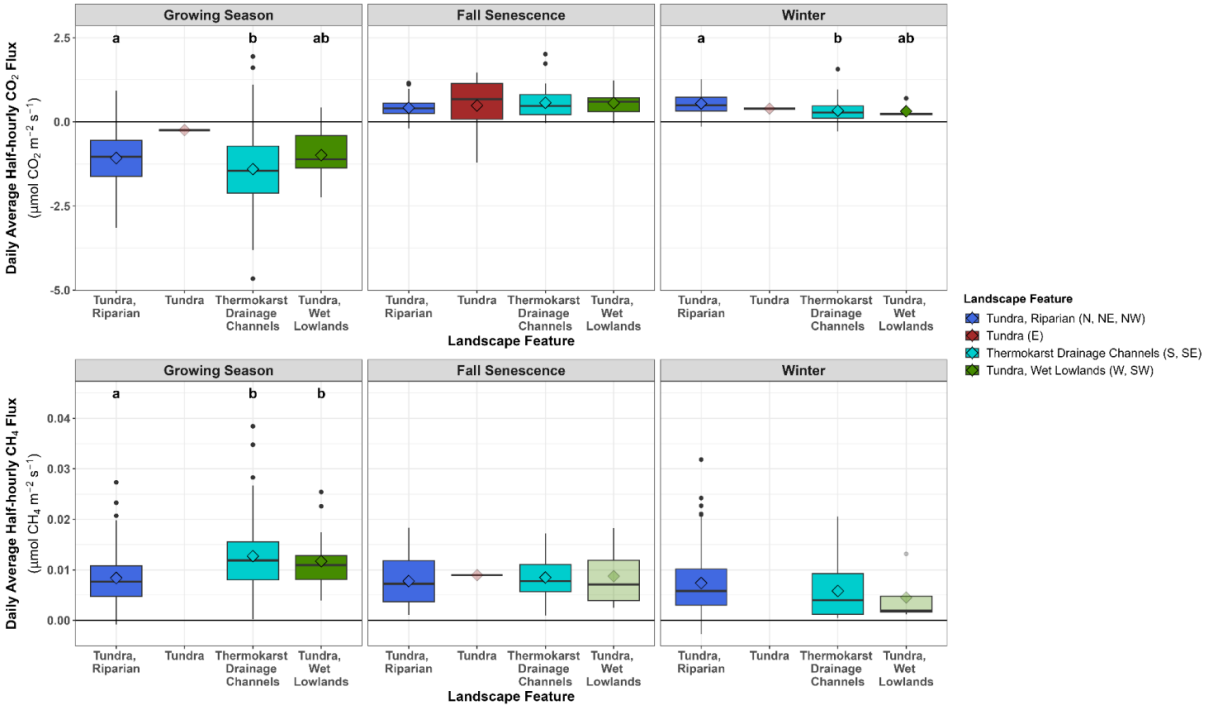

Figure 5. Daily mean CO_2 flux and daily mean CH_4 flux by winds from various landscape features during growing season, fall senescence, and winter. Reduced opacity indicates landscape features with less than five wind direction observations, therefore excluded from statistical analyses. Letters represent wind directions within each season with statistically significant differences in carbon fluxes at $p < 0.05$.

3.5 Flux Chamber Carbon Fluxes

3.5.1 Variation in Environmental Factors among Landscape Positions and Inundation

Overall, lowland landscape positions exhibited the highest mean soil temperatures (7.4 ± 0.5 ºC), highest mean air temperatures (16.18 ± 0.80 ºC), deepest mean thaw depth (54 ± 4 cm), and highest mean soil moisture (50.9 ± 3.1 %) among landscape positions during the study period (Table 2; Fig. S25). Mean soil and air temperature were similar among landscape positions (Table 2), but upland positions had significantly ($p < 0.001$) lower mean thaw depth (39 ± 2 cm) compared to lowland positions (54 ± 4 cm). Mean soil moisture was also significantly lower ($p < 0.001$) in both upland (33.3 ± 2.5 %) and slope (30.1 ± 5.5 %) positions compared to lowland plots (Table 2; Fig. S25).

https://doi.org/10.5194/egusphere-2026-3328
Preprint. Discussion started: 3 July 2026

Differences among landscape positions, however, were largely impacted by inundation status. There were no significant differences among inundated landscape positions. Yet, data suggest inundated lowland plots may have higher mean soil and air temperatures as well as deeper mean thaw depth compared to inundated upland plots, whereas inundated upland plots recorded higher mean soil moisture compared to inundated lowland plots (Table 2; Fig. S25). When not inundated, there were no significant differences in mean soil and air temperature among landscape positions, but the lowland position featured significantly ($p = 0.01$) deeper mean thaw depth (50 ± 4 cm) compared to upland positions (37 ± 2 cm) and significantly higher mean soil moisture (45.3 ± 3.0 %) compared to both slope (30.1 ± 5.5 %; $p = 0.01$) and upland (30.7 ± 2.3 %; $p < 0.002$) positions. Additionally, there were also significant differences between inundated and non-inundated landscape positions. Inundated lowland positions had significantly higher soil temperature ($p=0.017$), thaw depth ($p = 0.047$), and soil moisture ($p = 0.002$) compared to non-inundated lowland plots. Similarly, upland landscape positions that were inundated had significantly deeper thaw depth ($p = 0.004$) and higher soil moisture ($p = 0.004$) compared to non-inundated upland positions (Table 2; Fig. S25).

Table 2. Average (± SE) of flux chamber measurements of NEE, GPP, RECO (μmol C m^{-2} s^{-1}), and CH_4 fluxes (nmol C m^{-2} s^{-1}), as well as environmental variables of interest, by landscape position and inundation. Only means with n > 5 observations reported. Measurements were taken from the 35 soil chambers intermittently during the months of June, July, August, and September of 2016 through 2019.

Flux Chamber Measurement Means by Landscape Position										
Landscape Position	Inundated	NEE (μmol CO_2 m^{-2} s^{-1})	GPP (μmol CO_2 m^{-2} s^{-1})	RECO (μmol CO_2 m^{-2} s^{-1})	CH_4 Flux (nmol CH_4 m^{-2} s^{-1})	Thaw depth (cm)	SWC (%)	10 cm Soil Temperature (°C)	Air Temperature (°C)	n
lowland	-	-0.41 ± 0.17	1.84 ± 0.23	1.43 ± 0.13	32.6 ± 7.72	54 ± 4	50.9 ± 3.1	7.4 ± 0.5	16.18 ± 0.80	46
slope	-	-0.10 ± 0.24	1.63 ± 0.25	1.53 ± 0.2	22.65 ± 12.73	43 ± 4	30.1 ± 5.5	6.9 ± 0.8	14.47 ± 1.26	21
upland	-	-0.66 ± 0.21	2.16 ± 0.22	1.50 ± 0.11	17.88 ± 6.5	39 ± 2	33.3 ± 2.5	6.9 ± 0.4	15.70 ± 0.60	85
Flux Chamber Measurement Means by Landscape Position and Inundation Status										
lowland	N	-0.39 ± 0.21	1.8 ± 0.28	1.42 ± 0.15	12.47 ± 3.42	50 ± 4	45.3 ± 3.0	6.7 ± 0.5	15.95 ± 0.97	33
lowland	Y	-0.47 ± 0.24	1.93 ± 0.41	1.47 ± 0.25	83.68 ± 20.24	66 ± 5	65.2 ± 6.4	9.4 ± 0.9	16.78 ± 1.46	13
slope	N	-0.10 ± 0.24	1.63 ± 0.25	1.53 ± 0.2	22.65 ± 12.73	43 ± 4	30.1 ± 5.5	6.9 ± 0.8	14.47 ± 1.26	21
upland	N	-0.66 ± 0.23	2.15 ± 0.24	1.49 ± 0.11	6.78 ± 4.57	37 ± 2	30.7 ± 2.3	6.9 ± 0.4	15.82 ± 0.61	79
upland	Y	-0.72 ± 0.49	2.34 ± 0.26	1.62 ± 0.25	164.15 ± 34.39	63 ± 8	67.8 ± 10.8	7.3 ± 1.0	14.12 ± 2.94	6

3.5.2 Variation in Chamber Carbon Fluxes among Landscape Positions and Inundation

There were no significant differences in mean GPP, R_{ECO}, or NEE among landscape positions or inundation status, though data suggest there may be a pattern. Generally, NEE, GPP, and R_{ECO} fluxes were greater on upland landscape positions compared to lowland landscape positions, and fluxes were also greater if the landscape position was inundated compared to non-inundated, with the greatest mean NEE, GPP, and R_{ECO} measured from inundated upland plots (Table 2; Fig. 6). All landscape positions (upland, slope, lowland), both inundated and non-inundated, indicated mean net carbon uptake (negative NEE values) during the study period.

There were, however, significant differences in CH_4 fluxes among landscape positions, where mean CH_4 emissions were significantly higher in lowland landscape positions (32.6 ± 7.72 nmol CH_4 m^{-2} s^{-1}) compared to slope (22.65 ± 12.73 nmol CH_4 m^{-2} s^{-1}; $p = 0.002$) and upland (17.88 ± 6.5 nmol CH_4 m^{-2} s^{-1}; $p < 0.001$) positions (Table 2; Fig. 6).

https://doi.org/10.5194/egusphere-2026-3328
Preprint. Discussion started: 3 July 2026

When partitioned by inundation status, mean non-inundated lowland emissions (12.47 ± 3.42 nmol CH_4 m^{-2} s^{-1}) were significantly higher (p = 0.002) than non-inundated upland emissions (6.78 ± 4.57 nmol CH_4 m^{-2} s^{-1}) but also significantly lower (p = 0.03) than mean fluxes from slope positions (22.65 ± 12.73 nmol CH_4 m^{-2} s^{-1}) (Table 2; Fig. 7). When inundated, mean CH_4 emissions were roughly twice as high from the inundated upland position (164.15 ± 34.39 nmol CH_4 m^{-2} s^{-1}) compared to the inundated lowland position (83.68 ± 20.24 nmol CH_4 m^{-2} s^{-1}), though due to the high variability, the difference in means was not significant (p = 0.6). In both upland and lowland positions, CH_4 fluxes were significantly greater when inundated compared to when not inundated ($p<0.001$ and $p<0.001$, respectively) (Fig. 7).

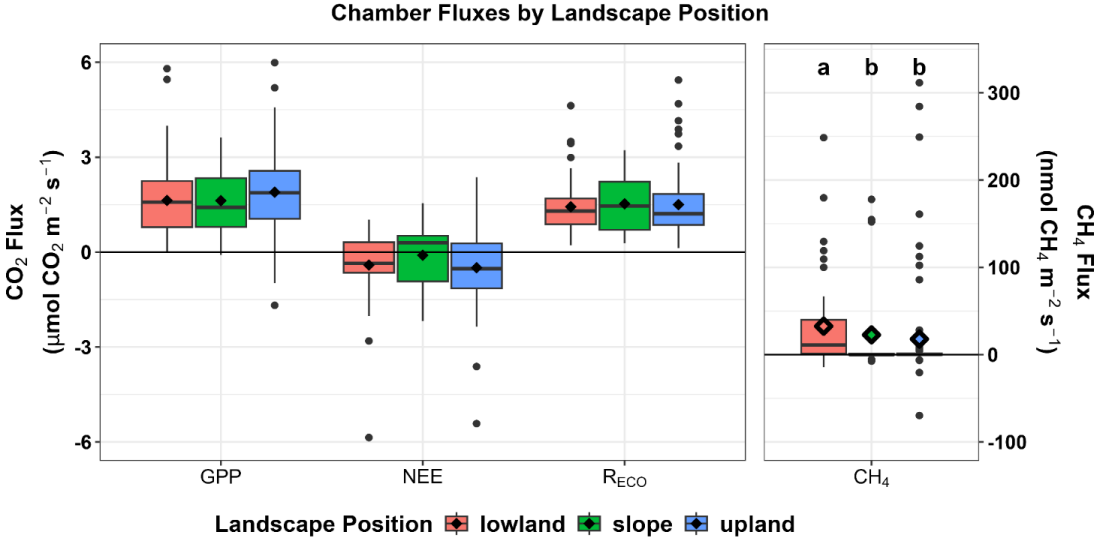

Figure 6. Mean gross primary production (GPP), net ecosystem exchange (NEE), ecosystem respiration (R_{ECO}), and methane (CH_4) measured by flux chambers placed in various landscape positions (lowland, slope, upland) around the study site at Council, AK. The bold line represents the median; the diamond represents the mean over the study period. The different letters in the CH_4 figure panel represent statistically significant differences in fluxes among landscape positions at $p < 0.05$.

https://doi.org/10.5194/egusphere-2026-3328
Preprint. Discussion started: 3 July 2026

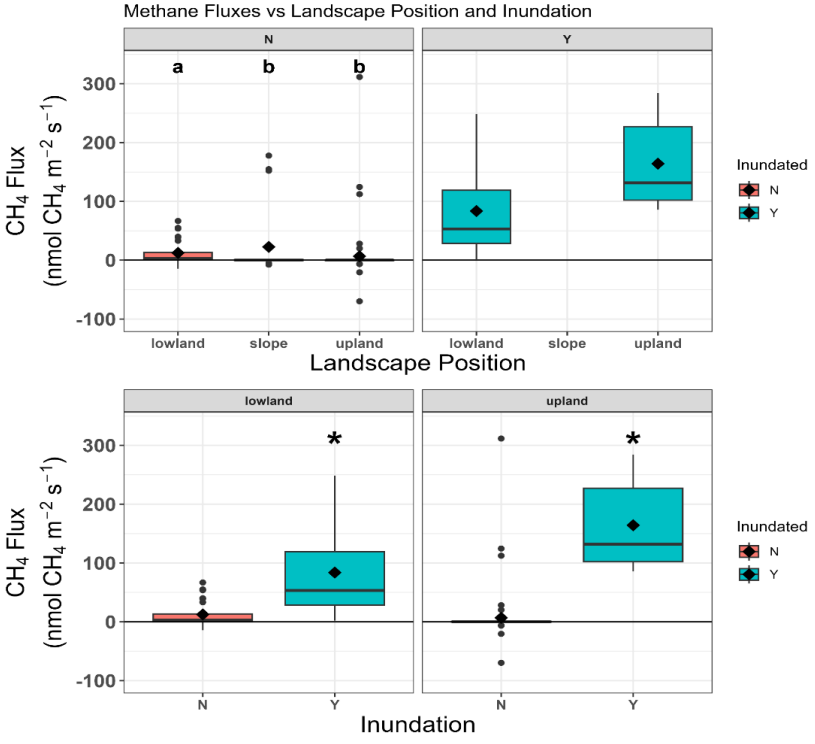

Figure 7. Methane fluxes measured by flux chambers placed in various landscape positions (lowland, slope, upland) that were either inundated (turquoise) or not inundated (red). The bold line represents the median; the black diamond represents the cumulative average. Different letters signify statistically different fluxes among landscape positions at $p<0.05$; a " * " denotes significantly higher fluxes when landscape positions were inundated compared to when they were not inundated at $p<0.05$.

4. Discussion

Overall, we found that the Council site was a net carbon source during the study period, with 2017 - 2018 being the only net carbon sink year. Higher net carbon emissions aligned with warmer temperatures and wetter conditions during the first three years of the study; the net carbon source was lower with cooler and drier conditions in subsequent years. While temperature and soil moisture were important factors for carbon fluxes, thermokarst landscape features and microtopography were also important drivers of carbon fluxes. There were significant differences in CO_2 and CH_4 fluxes when winds came from thermokarst drainage channels to the south of the EC tower, and significant differences in CH_4 chamber fluxes based on landscape position and inundation.

4.1 Interannual Variability of EC Tower Carbon and Meteorological Measurements

Based on 2018 - 2019 seasonal measurements, mean daily CH_4 winter fluxes could be ~ 44% of the daily average growing season fluxes and mean daily CO_2 winter fluxes could be up to ~ 45% of the daily average growing season

https://doi.org/10.5194/egusphere-2026-3328
Preprint. Discussion started: 3 July 2026

fluxes. These percentages are comparable to R_{ECO} offset of summer CO_2 uptake and winter CH_4 emissions measured at other Arctic tundra sites (Arndt et al., 2020; Raz-Yaseef et al., 2017; Zona et al., 2016). Due to the length of the winter period, winter CO_2 and CH_4 emissions alone were nearly as high or higher than growing period CO_2 uptake and summer CH_4 emissions, consistent with other studies that concluded winter carbon emissions can make up a substantial portion of annual carbon budgets (Arndt et al., 2020; Natali et al., 2019; Raz-Yaseef et al., 2017; Zona et al., 2016). These proportionate budgets were more conservative than random forest gap-filled budgets, which produced roughly 9% to 46% greater total annual winter carbon emissions compared to the winter-proportion approach (Table S4). Still, these adjusted winter budgets should be taken with consideration of the limitations and interannual variability, and should be viewed as a potential benchmark to reassess in future studies when more winter CO_2 and CH_4 data may be available.

The largest carbon source years also had relatively high mean growing season and fall air temperature, soil temperature, and soil moisture, as well as higher relative humidity with lower mean vapor pressure deficit compared to latter years. These years also had comparatively short growing seasons and winters, but long fall periods that resulted in the highest fall carbon emissions among years (Table 1). The longest fall season (2020), however, did not yield the highest fall carbon emissions; it was notably cooler compared to fall in 2018 and 2019. Winters were also notably warmer in 2017/2018 and 2018/2019, likely contributing to the high net carbon emissions of 2019/2020. This suggests that interannual variability in seasonal temperatures and soil moisture may be more influential over carbon budgets than season length. After the 2019-2020 winter ended, mean annual carbon budgets decreased over tenfold, concomitant with a pattern of lower seasonal mean soil moisture and lower seasonal mean air and soil temperatures, which can limit respiration and stymie CH_4 emissions (Lu et al., 2022). Soil moisture impacts nutrient distribution and availability as well, thereby controlling microbial and plant uptake and productivity (López-Blanco et al., 2020; Rustad et al., 2001; Shaver and Chapin, 1980). The drier ambient air conditions in the latter years of the study period could also indicate greater evapotranspiration, further facilitating moisture loss. These findings underscore the need for longer-term *in situ* measurements that can capture carbon flux response to interannual variability due to shorter-term weather trends – such as uncharacteristically warm, cool, wet or dry years – as well as longer-term climate trajectories.

4.2 Variable Importance for EC Carbon Fluxes

Arctic studies show that temperature and moisture are key regulating factors for seasonal CO_2 and CH_4 emissions (Lu et al., 2022; Rustad et al., 2001; Voigt et al., 2017). Warmer seasons stimulate plant growth and respiration, and enhance microbial respiration, yielding greater CO_2 uptake but also greater carbon emissions. Additionally, saturated soils correlate with greater CH_4 emissions due to anaerobic conditions that promote methanogenesis (Liblik et al., 1997; Voigt et al., 2017). Yet, we did not find significant correlations between seasonal means of predictor variables and carbon budgets across years, and the significant correlations between daily means of growing season CO_2 fluxes and temperature variables, as well as between daily means of growing season CH_4 fluxes and temperature and moisture variables, were very weak.

https://doi.org/10.5194/egusphere-2026-3328
Preprint. Discussion started: 3 July 2026

The weak relationships may stem from various years having large data gaps and high variability among years, stressing the need for longer-term data to validate and better characterize these relationships. Results may have been further impacted by the placement of the soil temperature and soil moisture sensors, which could have led to a decoupling between growing season soil temperature / moisture and carbon flux response. The exponential relationship between nighttime CO_2 fluxes (Fig. 8) and R_{ECO} (Fig. S22) with soil temperature followed expectations that as temperatures increase, so does respiration (Rustad et al., 2001). However, when winter was included, daily mean CH_4 fluxes exhibited a weak, but significant U-shaped parabolic relationship with measured soil temperature (Fig. S10), representing high winter CH_4 emissions when measured soil temperatures were roughly between -9 °C and -3 °C. This pattern was predominantly driven by daily mean measurements from the fall in 2019 (November 13 - 25, 2019). The highest CH_4 emissions during this period occurred when soil temperatures were coldest, possibly signaling a CH_4 burst from frozen soil cracking and releasing trapped gasses rather than a biological source.

Other studies have also found that temperature and moisture conditions do not always directly translate to predictable variability in carbon fluxes. For example, while satellite imagery indicates widespread increases in plant productivity in northern latitudes due to warming (Berner et al., 2020; Guay et al., 2014), some studies found this hasn't yielded parallel increases in summer carbon uptake. Atmospheric CO_2 measurements have shown a weakening summer CO_2 sink in past decades (Piao et al., 2014; Wang et al., 2018). An EC study by Zona et al. (2023) found decreased GPP in response to higher temperatures during peak summer (July) at various circumpolar sites due to soil moisture limitations on plant productivity. Carbon flux measurements from another EC site near Council, Alaska found evidence that temperature sensitivity for R_{ECO} was higher than for GPP for most of the growing season, and data pointed toward non-linear relationships between GPP, R_{ECO}, and temperature (Lee et al., 2024). Similar studies concluded that differences in growing season CH_4 fluxes were not explained by changes in typical driving factors such as soil temperature and soil moisture, rather, CH_4 fluxes were related to the date of snowmelt (Mastepanov et al., 2013) or linked to gas production from the prior fall season (Raz-Yaseef et al., 2017). These findings point toward a complex dynamic between temperature, moisture, biogeochemical processes, and carbon fluxes, and support the assertion that drivers of Arctic carbon fluxes can be spatiotemporally variable on local to landscape scales.

4.3 Impact of Landscape Features on EC Carbon Fluxes

Nearby landscape features – distinguished within the EC footprint by different prevailing wind directions – had significant impacts on both CO_2 and CH_4 fluxes and may have an outsized influence on carbon flux variability at the Council site. Thermokarst features, such as the thermoerosional drainage channels / gullies south of the EC tower, tend to be the result of abrupt thaw events that collapse ground ice in the permafrost (Jorgenson et al., 2006). This causes the ground to subside and increases heat flux into the ground via water impoundment or transportation, snow accumulation, and changes in vegetation cover (Jorgenson and Osterkamp, 2005; Kokelj and Jorgenson, 2013; Osterkamp et al., 2009). These processes can restructure landscape geomorphology, altering soil properties, organic matter composition, nutrient distribution, hydrology, topography, and microbial communities, modifying carbon

https://doi.org/10.5194/egusphere-2026-3328
Preprint. Discussion started: 3 July 2026

dynamics. Our findings highlighted significantly greater CO_2 uptake and higher CH_4 emissions from the southern thermokarst drainage channels during the growing season (Fig. 5). Alternatively, during the winter, there were significantly greater CO_2 emissions detected from the northern tundra bordering the riparian areas compared to the southern thermokarst drainage channels. This suggests that the thermokarst drainage channels are a greater CO_2 sink and CH_4 source during the growing season and a weaker CO_2 source during the winter compared to the surrounding tundra landscape. These opposing seasonal patterns may be explained by the various impacts thermokarst can have on landscape processes, mediated by environmental conditions during different seasons.

During warm periods such as the growing season, thermal erosion exposes deeper, carbon-rich soils to microbial decomposition (Estop-Aragonés et al., 2020), making carbon and other nutrients available for uptake, transport, or emission. A study by Wang et al. (2024) observed that warming-induced CO_2 release was ~5.5 times higher in dry, upland thermokarst features compared to non-thermokarst landforms due to differences in soil organic matter and microbial communities. Thermokarst could therefore trigger a positive feedback to warming. Furthermore, warmer soil temperatures in thermokarst features (Schuur et al., 2007) and anoxic, saturated soils promote methanogenesis (Lai, 2009), enhancing methane production in subsided thermokarst formations. Thermokarst features that impound water have been observed to act as CH_4 hotspots and thaw ponds are often recorded as being high emitters of both CO_2 and CH_4 (Kuhn et al., 2018). Such hotspots are capable of offsetting carbon sink capabilities by ~ 39%, though this is highly dependent on the extent of thermokarst, inundation, and vegetation (Kuhn et al., 2018). For example, hydrophytic and wetland vegetation growing in saturated, anoxic soils use aerenchymatous tissues to transport oxygen from the roots to the shoots, a pathway that can also transport CH_4 from the soils to the atmosphere. Plant-mediated CH_4 transport can significantly increase ecosystem CH_4 emissions (Andresen et al., 2017; Noyce et al., 2014). Conversely, remobilization of nutrients and elevated soil moisture in thermokarst gullies can promote plant growth uninhibited by water stress, increasing CO_2 uptake during the growing season (Rodenhizer et al., 2022), thereby partially offsetting carbon losses. At Council, measurements show greater mean growing season CH_4 emissions associated with the thermokarst drainage channels, but the concomitant elevated mean CO_2 uptake was orders of magnitude greater; the thermokarst drainage channels were a net carbon sink during the study period.

During cold periods, thermokarst formations may enhance respiration but also stymie outgassing due to the insulating effects of snowpack. At Council, the thermokarst channels exhibited lower carbon emissions during the winter compared to the tundra bordering the riparian area to the north of the tower. Deeper snowpack has been shown to insulate the soil, maintain higher winter temperatures, and promote microbial activity and carbon loss (Pedron et al., 2023). Snowpack in the thermo-erosional gullies at Council, however, may be sheltered and become compacted enough to trap and store carbon emissions during the winter, thus appearing to have reduced winter emissions. These findings reflect the spatiotemporally diverse impacts thermokarst features can have on carbon dynamics. The identifiable influence of surrounding landscape features on measured EC carbon fluxes can help researchers better parameterize the complex, ecologically mediated biogeochemical processes that drive carbon cycling in the Arctic. This, in turn, can inform model extrapolations across heterogeneous Arctic landscapes.

https://doi.org/10.5194/egusphere-2026-3328
Preprint. Discussion started: 3 July 2026

4.4 Impact of Microtopography and Inundation on Flux Chamber Measurements

As with thermokarst topography, landscape microtopography generates great spatial heterogeneity in abiotic conditions, thereby also creating spatial variation in ecosystem processes (Bockheim et al., 1999; Walker et al., 2008; Zona et al., 2011). Soil features, moisture, temperature, and nutrients can vary greatly among different microtopographical features (Bockheim et al., 1999; Walker et al., 2008), driving spatial heterogeneity in carbon fluxes on local scales. Over the study period, chamber flux measurements showed significantly higher mean soil moisture and significantly deeper mean thaw depth in lowland landscape positions compared to upland landscape positions, especially when inundated (Table 2). Inundated landscape positions featured significantly higher mean soil moisture and significantly deeper mean thaw depth (Fig. S25) compared to non-inundated landscape positions, which could indicate higher nutrient availability due to permafrost thaw and hydrologic transport of nutrients. Inundated lowland landscape positions also had significantly warmer mean soil temperature compared to non-inundated lowland positions.

However, we detected no significant differences in mean chamber flux measurements of R_{ECO}, GPP, and NEE among landscape positions during the study period, though there were observable patterns. Regardless of inundation, upland landscape positions had marginally greater respiration, were more productive, and behaved as stronger carbon sinks compared to lowland positions (Table 2; Fig. 6), coinciding with significantly drier soils and significantly shallower mean thaw depth (Table 2; Fig. S25). Inundation also tended to increase GPP and R_{ECO} in both lowland and upland positions, thereby increasing the NEE sink, exemplifying how soil moisture can enhance both productivity and respiration (Table 2). The impact of inundation was particularly pronounced in chamber flux measurements of CH_4.

We found significant differences in CH_4 fluxes among landscape positions and inundation status, supporting findings of elevated CH_4 emissions from low, wet areas (such as seen from the thermokarst drainage channels). Regardless of inundation, lowland landscape positions had higher overall mean CH_4 emissions compared to slope and upland positions (Fig. 6). When not inundated, CH_4 emissions were significantly higher in lowland landscape positions compared to upland and slope positions (Fig. 7; Table 2), aligning with significantly higher soil moisture and significantly deeper mean thaw depths. As the mean air and soil temperatures were similar, this difference in emissions is likely influenced more by soil moisture and thaw depth than by temperature. This was further exemplified by finding significantly greater mean CH_4 emissions from both lowland and upland positions when the plots were inundated compared to non-inundated, whereas there were no significant differences between upland and lowland landscape positions when they were both inundated (Fig. 7). The inundated upland landscape position had highest mean CH_4 emissions among all landscape types, roughly 1.5 times the emissions from the inundated lowland position, despite the lowland landscape position featuring deeper mean thaw depth and higher mean soil and air temperatures. The non-inundated upland landscape position had one of the lowest mean soil moisture levels among landscape positions, possibly indicating water stress that was alleviated by periodic inundation. Additionally, when upland tundra soils become temporarily anoxic due to saturation, methanogenesis (Liblik et al., 1997; Voigt et al., 2017) and plant-mediated transport may facilitate higher CH_4 emissions (Andresen et al., 2017; Noyce et al., 2014).

https://doi.org/10.5194/egusphere-2026-3328
Preprint. Discussion started: 3 July 2026

These findings have important implications for characterizing differences in ecological conditions that drive spatiotemporal variability in carbon fluxes. The flux chambers support results from the EC tower measurements indicating heightened CH_4 emissions from wet, low areas with deeper thaw depths, conditions also present in thermoerosional gullies and thermokarst drainage channels. However, these data also highlight that periodically inundated upland tundra areas can emit CH_4 at rates than can potentially exceed wet, lowland features typically considered CH_4 emission hotspots (Elder et al., 2021; Kuhn et al., 2018; Laurion et al., 2010). More research is needed to explore the influence ephemerally inundated upland tundra sites may exert on carbon fluxes. Identifying these parallels and divergences can allow researchers to draw inferences from smaller-scale studies for parameterizing carbon fluxes on larger scales based on landscape features and microtopography.

5. Conclusion

Long-term monitoring of changing environmental conditions and the response in carbon fluxes in Council, AK can offer valuable insight into how future northern Arctic ecosystems may behave, and how carbon sink and source capabilities may evolve with a warming Arctic. This analysis of a six-year EC record provides a baseline for longer-term monitoring and future comparisons of carbon flux responses to changing environmental conditions. Interannual variability in annual and seasonal temperatures and soil moisture aligned with carbon source and sink strength. Steep increases in net carbon emissions mirrored warmer temperatures and wetter conditions, followed by steep decreases in net carbon emissions during years with cooler temperatures and drier conditions. While temperature and soil moisture were identified as important variables for carbon fluxes, landscape features – such as thermokarst and microtopography – also significantly impact carbon emissions at Council. Conditions created by thermokarst and landscape microtopography can promote both carbon emission and carbon uptake through processes that are mediated by varying seasonal environmental conditions. Such processes may also be heavily impacted by inundation, even if only ephemerally inundated. These nuances in carbon dynamics based not only on meteorological conditions, but also microtopography and landscape features, need to be considered when modeling Arctic carbon dynamics.

Data Availability

Eddy covariance tower data is publicly available on the Ameriflux database (https://ameriflux.lbl.gov/) under site ID "US-NGC" (doi: 10.17190/AMF/1634883) (Torn and Dengel, 2020).

Meteorological and ancillary data can be accessed through the NGEE Arctic data portal (https://ngee-arctic.ornl.gov) at https://doi.org/10.5440/1526749 (Dengel and Torn, 2020).

Flux chamber data is publicly available on the ESS-DIVE website (https://ess-dive.lbl.gov) and can be accessed at: doi:10.5440/1765733.

https://doi.org/10.5194/egusphere-2026-3328
Preprint. Discussion started: 3 July 2026

Supplement

(Supplemental file attached.)

Author contributions

Conceptualization: KK, KA, SD, MT, SN; Data curation: SD, MT, OC; Formal Analysis: KK, KA; Funding: KA, SN, DT, MT; Investigation: all coauthors; Methodology: KK, KA, SD, MT, SN; Project Administration: MT, SD, KA, SN, KK; Resources: SD, MT, OC, SN, KA, KK; Software: SD, MT, KA, KK; Supervision: SN, KA; Visualization: KK; Writing – original draft: KK; Writing – review and editing: all co-authors.

Competing interests

None of the authors have any competing interests.

Disclaimer

Copernicus Publications remains neutral with regard to jurisdictional claims made in the text, published maps, institutional affiliations, or any other geographical representation in this paper. While Copernicus Publications makes every effort to include appropriate place names, the final responsibility lies with the authors. Views expressed in the text are those of the authors and do not necessarily reflect the views of the publisher.

Acknowledgements

We thank the Next-Generation Ecosystem Experiments (NGEE Arctic) project – supported by the Office of Biological and Environmental Research in the DOE Office of Science – for the installation and maintenance of the EC tower and flux chambers used in this study.

Financial support

This research was supported by the TED x Audacious grant awarded to Dr. Sue Natali for the “Permafrost Pathways” project implemented by Woodwell Climate Research Center in Falmouth, MA, USA.

https://doi.org/10.5194/egusphere-2026-3328
Preprint. Discussion started: 3 July 2026

References

Abbott, B. W. and Jones, J. B.: Permafrost collapse alters soil carbon stocks, respiration, CH_4, and N_2O in upland tundra, Glob. Change Biol., 21, 4570–4587, https://doi.org/10.1111/gcb.13069, 2015.

Abbott, B. W., Jones, J. B., Godsey, S. E., Larouche, J. R., and Bowden, W. B.: Patterns and persistence of hydrologic carbon and nutrient export from collapsing upland permafrost, Biogeosciences, 12, 3725–3740, https://doi.org/10.5194/bg-12-3725-2015, 2015.

Abolt, C. J., Young, M. H., Atchley, A. L., Harp, D. R., and Coon, E. T.: Feedbacks Between Surface Deformation and Permafrost Degradation in Ice Wedge Polygons, Arctic Coastal Plain, Alaska, J. Geophys. Res. Earth Surf., 125, e2019JF005349, https://doi.org/10.1029/2019JF005349, 2020.

Andresen, C. G., Lara, M. J., Tweedie, C. E., and Lougheed, V. L.: Rising plant-mediated methane emissions from arctic wetlands, Glob. Change Biol., 23, 1128–1139, https://doi.org/10.1111/gcb.13469, 2017.

Arndt, K. A., Oechel, W. C., Goodrich, J. P., Bailey, B. A., Kalhori, A., Hashemi, J., Sweeney, C., and Zona, D.: Sensitivity of Methane Emissions to Later Soil Freezing in Arctic Tundra Ecosystems, J. Geophys. Res. Biogeosciences, 124, 2595–2609, https://doi.org/10.1029/2019JG005242, 2019.

Arndt, K. A., Lipson, D. A., Hashemi, J., Oechel, W. C., and Zona, D.: Snow melt stimulates ecosystem respiration in Arctic ecosystems, Glob. Change Biol., 26, 5042–5051, https://doi.org/10.1111/gcb.15193, 2020.

Berner, L. T., Massey, R., Jantz, P., Forbes, B. C., Macias-Fauria, M., Myers-Smith, I., Kumpula, T., Gauthier, G., Andreu-Hayles, L., Gaglioti, B. V., Burns, P., Zetterberg, P., D'Arrigo, R., and Goetz, S. J.: Summer warming explains widespread but not uniform greening in the Arctic tundra biome, Nat. Commun., 11, 4621, https://doi.org/10.1038/s41467-020-18479-5, 2020.

Biskaborn, B. K., Smith, S. L., Noetzli, J., Matthes, H., Vieira, G., Streletskiy, D. A., Schoeneich, P., Romanovsky, V. E., Lewkowicz, A. G., Abramov, A., Allard, M., Boike, J., Cable, W. L., Christiansen, H. H., Delaloye, R., Diekmann, B., Drozdov, D., Etzelmüller, B., Grosse, G., Guglielmin, M., Ingeman-Nielsen, T., Isaksen, K., Ishikawa, M., Johansson, M., Johannsson, H., Joo, A., Kaverin, D., Kholodov, A., Konstantinov, P., Kröger, T., Lambiel, C., Lanckman, J.-P., Luo, D., Malkova, G., Meiklejohn, I., Moskalenko, N., Oliva, M., Phillips, M., Ramos, M., Sannel, A. B. K., Sergeev, D., Seybold, C., Skryabin, P., Vasiliev, A., Wu, Q., Yoshikawa, K., Zheleznyak, M., and Lantuit, H.: Permafrost is warming at a global scale, Nat. Commun., 10, 264, https://doi.org/10.1038/s41467-018-08240-4, 2019.

Bockheim, J. G., Everett, L. R., Hinkel, K. M., Nelson, F. E., and Brown, J.: Soil Organic Carbon Storage and Distribution in Arctic Tundra, Barrow, Alaska, Soil Sci. Soc. Am. J., 63, 934–940, https://doi.org/10.2136/sssaj1999.634934x, 1999.

Cassidy, A. E., Christen, A., and Henry, G. H. R.: The effect of a permafrost disturbance on growing-season carbon-dioxide fluxes in a high Arctic tundra ecosystem, Biogeosciences, 13, 2291–2303, https://doi.org/10.5194/bg-13-2291-2016, 2016.

Chafe, O., Shirley, I., Wullschleger, S., and Torn, M.: Soil CO2 and CH4 Chamber Fluxes in Tussock Tundra, Council Road Mile Marker 71, Seward Peninsula, Alaska, 2016-2019, https://doi.org/10.5440/1765733, 2023.

Christiansen, H. H., Etzelmüller, B., Isaksen, K., Juliussen, H., Farbrot, H., Humlum, O., Johansson, M., Ingeman-Nielsen, T., Kristensen, L., Hjort, J., Holmlund, P., Sannel, A. B. K., Sigsgaard, C., Åkerman, H. J., Foged, N., Blikra, L. H., Pernosky, M. A., and Ødegård, R. S.: The thermal state of permafrost in the nordic area during the international polar year 2007–2009, Permafr. Periglac. Process., 21, 156–181, https://doi.org/10.1002/ppp.687, 2010.

https://doi.org/10.5194/egusphere-2026-3328
Preprint. Discussion started: 3 July 2026

Copernicus Climate Change Service, Climate Data Store, (2023): ERA5 hourly data on single levels from 1940 to present. Copernicus Climate Change Service (C3S) Climate Data Store (CDS). DOI: 10.24381/cds.adbb2d47 (Accessed on 16-Sep-2024)

Dengel, S. and Torn, M.: NGEE Arctic CO2, CH4 and Energy Eddy-Covariance (EC) Flux Tower Auxiliary Measurements, Council Road Mile Marker 71, Seward Peninsula, Alaska, 2017 - 2019, https://doi.org/10.5440/1526749, 2020.

Dengel, S., Chafe, O., Cook, P., and Torn, M.: NGEE Arctic Soil Micro-warming Experiment Temperature Profiles, Council Road Mile Marker 71, Seward Peninsula, Alaska, 2017-2019, https://doi.org/10.5440/1634215, 2020.

Elder, C. D., Thompson, D. R., Thorpe, A. K., Chandanpurkar, H. A., Hanke, P. J., Hasson, N., James, S. R., Minsley, B. J., Pastick, N. J., Olefeldt, D., Walter Anthony, K. M., and Miller, C. E.: Characterizing Methane Emission Hotspots From Thawing Permafrost, Glob. Biogeochem. Cycles, 35, e2020GB006922, https://doi.org/10.1029/2020GB006922, 2021.

Elmendorf, S. C. and Hollister, R. D.: Limits on phenological response to high temperature in the Arctic, Sci. Rep., 13, 208, https://doi.org/10.1038/s41598-022-26955-9, 2023.

Estop-Aragonés, C., Olefeldt, D., Abbott, B. W., Chanton, J. P., Czimczik, C. I., Dean, J. F., Egan, J. E., Gandois, L., Garnett, M. H., Hartley, I. P., Hoyt, A., Lupascu, M., Natali, S. M., O'Donnell, J. A., Raymond, P. A., Tanentzap, A. J., Tank, S. E., Schuur, E. A. G., Turetsky, M., and Anthony, K. W.: Assessing the Potential for Mobilization of Old Soil Carbon After Permafrost Thaw: A Synthesis of ^{14}C Measurements From the Northern Permafrost Region, Glob. Biogeochem. Cycles, 34, e2020GB006672, https://doi.org/10.1029/2020GB006672, 2020.

Euskirchen, E. S., Edgar, C. W., Syndonia Bret-Harte, M., Kade, A., Zimov, N., and Zimov, S.: Interannual and Seasonal Patterns of Carbon Dioxide, Water, and Energy Fluxes From Ecotonal and Thermokarst-Impacted Ecosystems on Carbon-Rich Permafrost Soils in Northeastern Siberia, J. Geophys. Res. Biogeosciences, 122, 2651–2668, https://doi.org/10.1002/2017JG004070, 2017.

Foken, T., Göockede, M., Mauder, M., Mahrt, L., Amiro, B., and Munger, W.: Post-Field Data Quality Control, in: Handbook of Micrometeorology, vol. 29, edited by: Lee, X., Massman, W., and Law, B., Kluwer Academic Publishers, Dordrecht, 181–208, https://doi.org/10.1007/1-4020-2265-4_9, 2004.

Forster, P., T. Storelvmo, K. Armour, W. Collins, J.-L. Dufresne, D. Frame, D.J. Lunt, T. Mauritsen, M.D. Palmer, M. Watanabe, M. Wild, and H. Zhang, 2021: The Earth's Energy Budget, Climate Feedbacks, and Climate Sensitivity. In Climate Change 2021: The Physical Science Basis. Contribution of Working Group I to the Sixth Assessment Report of the Intergovernmental Panel on Climate Change [Masson-Delmotte, V., P. Zhai, A. Pirani, S.L. Connors, C. Péan, S. Berger, N. Caud, Y. Chen, L. Goldfarb, M.I. Gomis, M. Huang, K. Leitzell, E. Lonnoy, J.B.R. Matthews, T.K. Maycock, T. Waterfield, O. Yelekçi, R. Yu, and B. Zhou (eds.)]. Cambridge University Press, Cambridge, United Kingdom and New York, NY, USA, pp. 923–1054, doi:10.1017/9781009157896.009.

Guay, K. C., Beck, P. S. A., Berner, L. T., Goetz, S. J., Baccini, A., and Buermann, W.: Vegetation productivity patterns at high northern latitudes: a multi-sensor satellite data assessment, Glob. Change Biol., 20, 3147–3158, https://doi.org/10.1111/gcb.12647, 2014.

Hamed, K. H. and Rao, A. R. A modified Mann-Kendall trend test for autocorrelated data. Journal of Hydrology, 204(1–4): 182–196. <doi:10.1016/S0022-1694(97)00125-X>, 1998.

Hersbach, H., Bell, B., Berrisford, P., Biavati, G., Horányi, A., Muñoz Sabater, J., Nicolas, J., Peubey, C., Radu, R., Rozum, I., Schepers, D., Simmons, A., Soci, C., Dee, D., Thépaut, J-N. (2023): ERA5 hourly data on single levels from 1940 to present. Copernicus Climate Change Service (C3S) Climate Data Store (CDS), DOI: 10.24381/cds.adbb2d47 (Accessed on 16-SEP-2024)

https://doi.org/10.5194/egusphere-2026-3328
Preprint. Discussion started: 3 July 2026

Hewitt, R. E., Taylor, D. L., Genet, H., McGuire, A. D., and Mack, M. C.: Below-ground plant traits influence tundra plant acquisition of newly thawed permafrost nitrogen, J. Ecol., 107, 950–962, https://doi.org/10.1111/1365-2745.13062, 2019.

Hoffman, F. M., Kumar, J., Mills, R. T., and Hargrove, W. W.: Representativeness-based sampling network design for the State of Alaska, Landsc. Ecol., 28, 1567–1586, https://doi.org/10.1007/s10980-013-9902-0, 2013.

Hugelius, G., Strauss, J., Zubrzycki, S., Harden, J. W., Schuur, E. A. G., Ping, C.-L., Schirrmeister, L., Grosse, G., Michaelson, G. J., Koven, C. D., O'Donnell, J. A., Elberling, B., Mishra, U., Camill, P., Yu, Z., Palmtag, J., and Kuhry, P.: Estimated stocks of circumpolar permafrost carbon with quantified uncertainty ranges and identified data gaps, Biogeosciences, 11, 6573–6593, https://doi.org/10.5194/bg-11-6573-2014, 2014.

Hugelius, G., Loisel, J., Chadburn, S., Jackson, R. B., Jones, M., MacDonald, G., Marushchak, M., Olefeldt, D., Packalen, M., Siewert, M. B., Treat, C., Turetsky, M., Voigt, C., and Yu, Z.: Large stocks of peatland carbon and nitrogen are vulnerable to permafrost thaw, Proc. Natl. Acad. Sci., 117, 20438–20446, https://doi.org/10.1073/pnas.1916387117, 2020.

Jansson, J. K. and Taş, N.: The microbial ecology of permafrost, Nat. Rev. Microbiol., 12, 414–425, https://doi.org/10.1038/nrmicro3262, 2014.

Jorgenson, M. T. and Osterkamp, T. E.: Response of boreal ecosystems to varying modes of permafrost degradation, Can. J. For. Res., 35, 2100–2111, https://doi.org/10.1139/x05-153, 2005.

Jorgenson, M. T., Shur, Y. L., and Pullman, E. R.: Abrupt increase in permafrost degradation in Arctic Alaska, Geophys. Res. Lett., 33, 2005GL024960, https://doi.org/10.1029/2005GL024960, 2006.

Jorgenson, M. T., Romanovsky, V., Harden, J., Shur, Y., O'Donnell, J., Schuur, E. A. G., Kanevskiy, M., and Marchenko, S.: Resilience and vulnerability of permafrost to climate changeThis article is one of a selection of papers from The Dynamics of Change in Alaska's Boreal Forests: Resilience and Vulnerability in Response to Climate Warming., Can. J. For. Res., 40, 1219–1236, https://doi.org/10.1139/X10-060, 2010.

Jorgenson, M. T., Kanevskiy, M. Z., Jorgenson, J. C., Liljedahl, A., Shur, Y., Epstein, H., Kent, K., Griffin, C. G., Daanen, R., Boldenow, M., Orndahl, K., Witharana, C., and Jones, B. M.: Rapid transformation of tundra ecosystems from ice-wedge degradation, Glob. Planet. Change, 216, 103921, https://doi.org/10.1016/j.gloplacha.2022.103921, 2022.

Kanevskiy, M., Shur, Y., Jorgenson, T., Brown, D. R. N., Moskalenko, N., Brown, J., Walker, D. A., Raynolds, M. K., and Buchhorn, M.: Degradation and stabilization of ice wedges: Implications for assessing risk of thermokarst in northern Alaska, Geomorphology, 297, 20–42, https://doi.org/10.1016/j.geomorph.2017.09.001, 2017.

Kendall, M. Rank Correlation Methods. Griffin, London, 202 pp, 1975.

Kent, K., Trangmoe, D., and Lynoe, K.: Ecological Survey of Thaw Depth, Soil Organic Layer Thickness, Plant Functional Types, and Vegetation Height around an Eddy Covariance Tower at a Council, Alaska Tundra Site (June 2025), https://doi.org/10.18739/A2MW28H0H, 2026.

Kokelj, S. V. and Jorgenson, M. T.: Advances in Thermokarst Research, Permafr. Periglac. Process., 24, 108–119, https://doi.org/10.1002/ppp.1779, 2013.

Kuhn, M., Lundin, E. J., Giesler, R., Johansson, M., and Karlsson, J.: Emissions from thaw ponds largely offset the carbon sink of northern permafrost wetlands, Sci. Rep., 8, 9535, https://doi.org/10.1038/s41598-018-27770-x, 2018.

Lai, D. Y. F.: Methane Dynamics in Northern Peatlands: A Review, Pedosphere, 19, 409–421, https://doi.org/10.1016/S1002-0160(09)00003-4, 2009.

https://doi.org/10.5194/egusphere-2026-3328
Preprint. Discussion started: 3 July 2026

Laurion, I., Vincent, W. F., MacIntyre, S., Retamal, L., Dupont, C., Francus, P., and Pienitz, R.: Variability in greenhouse gas emissions from permafrost thaw ponds, Limnol. Oceanogr., 55, 115–133, https://doi.org/10.4319/lo.2010.55.1.0115, 2010.

Lee, H., Schuur, E. A. G., Vogel, J. G., Lavoie, M., Bhadra, D., and Staudhammer, C. L.: A spatially explicit analysis to extrapolate carbon fluxes in upland tundra where permafrost is thawing: EXTRAPOLATING ECOSYSTEM C FLUXES IN TUNDRA, Glob. Change Biol., 17, 1379–1393, https://doi.org/10.1111/j.1365-2486.2010.02287.x, 2011.

Lee, J.-Y., Chae, N., Kim, Y., Yun, J., Jeong, S., Choi, T., Kim, S.-J., Lee, B.-Y., and Park, S.-J.: Differential responses of respiration and photosynthesis to air temperature over a moist tundra ecosystem of Alaska and its impact on changing carbon cycle, Environ. Res. Commun., 6, 041003, https://doi.org/10.1088/2515-7620/ad3c17, 2024.

Liaw A and Wiener M 2022 Classification and regression by random Forest R News 2 18–22

Liblik, L. K., Moore, T. R., Bubier, J. L., and Robinson, S. D.: Methane emissions from wetlands in the zone of discontinuous permafrost: Fort Simpson, Northwest Territories, Canada, Glob. Biogeochem. Cycles, 11, 485–494, https://doi.org/10.1029/97GB01935, 1997.

López-Blanco, E., Jackowicz-Korczynski, M., Mastepanov, M., Skov, K., Westergaard-Nielsen, A., Williams, M., and Christensen, T. R.: Multi-year data-model evaluation reveals the importance of nutrient availability over climate in arctic ecosystem C dynamics, Environ. Res. Lett., 15, 094007, https://doi.org/10.1088/1748-9326/ab865b, 2020.

Lu, B., Song, L., Zang, S., and Wang, H.: Warming promotes soil CO2 and CH4 emissions but decreasing moisture inhibits CH4 emissions in the permafrost peatland of the Great Xing'an Mountains, Sci. Total Environ., 829, 154725, https://doi.org/10.1016/j.scitotenv.2022.154725, 2022.

Luo, G. J., Kiese, R., Wolf, B., and Butterbach-Bahl, K.: Effects of soil temperature and moisture on methane uptake and nitrous oxide emissions across three different ecosystem types, Biogeosciences, 10, 3205–3219, https://doi.org/10.5194/bg-10-3205-2013, 2013.

Lyu, Z. and Zhuang, Q.: Quantifying the Effects of Snowpack on Soil Thermal and Carbon Dynamics of the Arctic Terrestrial Ecosystems, J. Geophys. Res. Biogeosciences, 123, 1197–1212, https://doi.org/10.1002/2017JG003864, 2018.

Mann, H. B. Nonparametric Tests Against Trend. Econometrica, 13(3): 245-259, 1945.

Mar, K. A., Unger, C., Walderdorff, L., and Butler, T.: Beyond CO2 equivalence: The impacts of methane on climate, ecosystems, and health, Environ. Sci. Policy, 134, 127–136, https://doi.org/10.1016/j.envsci.2022.03.027, 2022.

Mastepanov, M., Sigsgaard, C., Tagesson, T., Ström, L., Tamstorf, M. P., Lund, M., and Christensen, T. R.: Revisiting factors controlling methane emissions from high-Arctic tundra, Biogeosciences, 10, 5139–5158, https://doi.org/10.5194/bg-10-5139-2013, 2013.

McGuire, A. D., Anderson, L. G., Christensen, T. R., Dallimore, S., Guo, L., Hayes, D. J., Heimann, M., Lorenson, T. D., Macdonald, R. W., and Roulet, N.: Sensitivity of the carbon cycle in the Arctic to climate change, Ecol. Monogr., 79, 523–555, https://doi.org/10.1890/08-2025.1, 2009.

McLeod, A. Kendall: Kendall Rank Correlation and Mann-Kendall Trend Test_. R package version 2.2.1, <https://CRAN.R-project.org/package=Kendall>, 2022.

Nadeem, I., Nakicenovic, N., Yaqub, A., Sakschewski, B., Loriani, S., Bala, G., Tharammal, T., and Zimm, C.: Permafrost Thawing and Estimates of Vulnerable Carbon in the Northern High Latitude, Earth Syst. Environ., 9, 715–740, https://doi.org/10.1007/s41748-024-00491-0, 2025.

https://doi.org/10.5194/egusphere-2026-3328
Preprint. Discussion started: 3 July 2026

Natali, S. M., Watts, J. D., Rogers, B. M., Potter, S., Ludwig, S. M., Selbmann, A.-K., Sullivan, P. F., Abbott, B. W., Arndt, K. A., Birch, L., Björkman, M. P., Bloom, A. A., Celis, G., Christensen, T. R., Christiansen, C. T., Commane, R., Cooper, E. J., Crill, P., Czimczik, C., Davydov, S., Du, J., Egan, J. E., Elberling, B., Euskirchen, E. S., Friborg, T., Genet, H., Göckede, M., Goodrich, J. P., Grogan, P., Helbig, M., Jafarov, E. E., Jastrow, J. D., Kalhori, A. A. M., Kim, Y., Kimball, J. S., Kutzbach, L., Lara, M. J., Larsen, K. S., Lee, B.-Y., Liu, Z., Loranty, M. M., Lund, M., Lupascu, M., Madani, N., Malhotra, A., Matamala, R., McFarland, J., McGuire, A. D., Michelsen, A., Minions, C., Oechel, W. C., Olefeldt, D., Parmentier, F.-J. W., Pirk, N., Poulter, B., Quinton, W., Rezanezhad, F., Risk, D., Sachs, T., Schaefer, K., Schmidt, N. M., Schuur, E. A. G., Semenchuk, P. R., Shaver, G., Sonnentag, O., Starr, G., Treat, C. C., Waldrop, M. P., Wang, Y., Welker, J., Wille, C., Xu, X., Zhang, Z., Zhuang, Q., and Zona, D.: Large loss of CO2 in winter observed across the northern permafrost region, Nat. Clim. Change, 9, 852–857, https://doi.org/10.1038/s41558-019-0592-8, 2019.

Natali, S. M., Holdren, J. P., Rogers, B. M., Treharne, R., Duffy, P. B., Pomerance, R., and MacDonald, E.: Permafrost carbon feedbacks threaten global climate goals, Proc. Natl. Acad. Sci., 118, e2100163118, https://doi.org/10.1073/pnas.2100163118, 2021.

Natali, S. M., Bronen, R., Cochran, P., Holdren, J. P., Rogers, B. M., and Treharne, R.: Incorporating permafrost into climate mitigation and adaptation policy, Environ. Res. Lett., 17, 091001, https://doi.org/10.1088/1748-9326/ac8c5a, 2022.

Noyce, G. L., Varner, R. K., Bubier, J. L., and Frolking, S.: Effect of *Carex rostrata* on seasonal and interannual variability in peatland methane emissions: EFFECT OF *C. ROSTRATA* ON CH_4 EMISSIONS, J. Geophys. Res. Biogeosciences, 119, 24–34, https://doi.org/10.1002/2013JG002474, 2014.

Oechel, W. C., Laskowski, C. A., Burba, G., Gioli, B., and Kalhori, A. A. M.: Annual patterns and budget of CO_2 flux in an Arctic tussock tundra ecosystem, J. Geophys. Res. Biogeosciences, 119, 323–339, https://doi.org/10.1002/2013JG002431, 2014.

Olefeldt, D., Goswami, S., Grosse, G., Hayes, D., Hugelius, G., Kuhry, P., McGuire, A. D., Romanovsky, V. E., Sannel, A. B. K., Schuur, E. A. G., and Turetsky, M. R.: Circumpolar distribution and carbon storage of thermokarst landscapes, Nat. Commun., 7, 13043, https://doi.org/10.1038/ncomms13043, 2016.

Osterkamp, T. E., Jorgenson, M. T., Schuur, E. A. G., Shur, Y. L., Kanevskiy, M. Z., Vogel, J. G., and Tumskoy, V. E.: Physical and ecological changes associated with warming permafrost and thermokarst in Interior Alaska, Permafr. Periglac. Process., 20, 235–256, https://doi.org/10.1002/ppp.656, 2009.

Panikov, N. S., Flanagan, P. W., Oechel, W. C., Mastepanov, M. A., and Christensen, T. R.: Microbial activity in soils frozen to below −39°C, Soil Biol. Biochem., 38, 785–794, https://doi.org/10.1016/j.soilbio.2005.07.004, 2006.

Pedron, S. A., Jespersen, R. G., Xu, X., Khazindar, Y., Welker, J. M., and Czimczik, C. I.: More Snow Accelerates Legacy Carbon Emissions From Arctic Permafrost, AGU Adv., 4, e2023AV000942, https://doi.org/10.1029/2023AV000942, 2023.

Piao, S., Nan, H., Huntingford, C., Ciais, P., Friedlingstein, P., Sitch, S., Peng, S., Ahlström, A., Canadell, J. G., Cong, N., Levis, S., Levy, P. E., Liu, L., Lomas, M. R., Mao, J., Myneni, R. B., Peylin, P., Poulter, B., Shi, X., Yin, G., Viovy, N., Wang, T., Wang, X., Zaehle, S., Zeng, N., Zeng, Z., and Chen, A.: Evidence for a weakening relationship between interannual temperature variability and northern vegetation activity, Nat. Commun., 5, 5018, https://doi.org/10.1038/ncomms6018, 2014.

Rantanen, M., Karpechko, A. Yu., Lipponen, A., Nordling, K., Hyvärinen, O., Ruosteenoja, K., Vihma, T., and Laaksonen, A.: The Arctic has warmed nearly four times faster than the globe since 1979, Commun. Earth Environ., 3, 168, https://doi.org/10.1038/s43247-022-00498-3, 2022.

Rao, A.R., Hamed,K.H.,&Chen,H.-L. Non-stationarities in hydrologic and environmental time series. Ringgold Inc., Portland, Oregon, 362 pp. <doi:10.1007/978-94-010-0117-5>, 2003.

https://doi.org/10.5194/egusphere-2026-3328
Preprint. Discussion started: 3 July 2026

Raz-Yaseef, N., Torn, M. S., Wu, Y., Billesbach, D. P., Liljedahl, A. K., Kneafsey, T. J., Romanovsky, V. E., Cook, D. R., and Wullschleger, S. D.: Large CO_2 and CH_4 emissions from polygonal tundra during spring thaw in northern Alaska, Geophys. Res. Lett., 44, 504–513, https://doi.org/10.1002/2016GL071220, 2017.

Rodenhizer, H., Belshe, F., Celis, G., Ledman, J., Mauritz, M., Goetz, S., Sankey, T., and Schuur, E. A. G.: Abrupt permafrost thaw accelerates carbon dioxide and methane release at a tussock tundra site, Arct. Antarct. Alp. Res., 54, 443–464, https://doi.org/10.1080/15230430.2022.2118639, 2022.

Romanovsky, V. E., Smith, S. L., and Christiansen, H. H.: Permafrost thermal state in the polar Northern Hemisphere during the international polar year 2007–2009: a synthesis, Permafr. Periglac. Process., 21, 106–116, https://doi.org/10.1002/ppp.689, 2010a.

Romanovsky, V. E., Drozdov, D. S., Oberman, N. G., Malkova, G. V., Kholodov, A. L., Marchenko, S. S., Moskalenko, N. G., Sergeev, D. O., Ukraintseva, N. G., Abramov, A. A., Gilichinsky, D. A., and Vasiliev, A. A.: Thermal state of permafrost in Russia, Permafr. Periglac. Process., 21, 136–155, https://doi.org/10.1002/ppp.683, 2010b.

Rustad, L., Campbell, J., Marion, G., Norby, R., Mitchell, M., Hartley, A., Cornelissen, J., and Gurevitch, J.: A meta-analysis of the response of soil respiration, net nitrogen mineralization, and aboveground plant growth to experimental ecosystem warming, Oecologia, 126, 543–562, https://doi.org/10.1007/s004420000544, 2001.

Salmabadi, H., Pardo Lara, R., Berg, A., Mavrovic, A., Hanes, C., Montpetit, B., and Roy, A.: Improving Seasonally Frozen Ground Monitoring Using Soil Freezing Characteristic Curve in Permittivity–Temperature Space, https://doi.org/10.5194/egusphere-2025-620, 15 May 2025.

Salmon, V. G., Soucy, P., Mauritz, M., Celis, G., Natali, S. M., Mack, M. C., and Schuur, E. A. G.: Nitrogen availability increases in a tundra ecosystem during five years of experimental permafrost thaw, Glob. Change Biol., 22, https://doi.org/10.1111/gcb.13204, 2016.

Schuur, E. A. G., Crummer, K. G., Vogel, J. G., and Mack, M. C.: Plant Species Composition and Productivity following Permafrost Thaw and Thermokarst in Alaskan Tundra, Ecosystems, 10, 280–292, https://doi.org/10.1007/s10021-007-9024-0, 2007.

Schuur, E. A. G., Bockheim, J., Canadell, J. G., Euskirchen, E., Field, C. B., Goryachkin, S. V., Hagemann, S., Kuhry, P., Lafleur, P. M., Lee, H., Mazhitova, G., Nelson, F. E., Rinke, A., Romanovsky, V. E., Shiklomanov, N., Tarnocai, C., Venevsky, S., Vogel, J. G., and Zimov, S. A.: Vulnerability of Permafrost Carbon to Climate Change: Implications for the Global Carbon Cycle, BioScience, 58, 701–714, https://doi.org/10.1641/B580807, 2008.

Schuur, E. A. G., McGuire, A. D., Schädel, C., Grosse, G., Harden, J. W., Hayes, D. J., Hugelius, G., Koven, C. D., Kuhry, P., Lawrence, D. M., Natali, S. M., Olefeldt, D., Romanovsky, V. E., Schaefer, K., Turetsky, M. R., Treat, C. C., and Vonk, J. E.: Climate change and the permafrost carbon feedback, Nature, 520, 171–179, https://doi.org/10.1038/nature14338, 2015.

Schuur, E. A. G., Abbott, B. W., Commane, R., Ernakovich, J., Euskirchen, E., Hugelius, G., Grosse, G., Jones, M., Koven, C., Leshyk, V., Lawrence, D., Loranty, M. M., Mauritz, M., Olefeldt, D., Natali, S., Rodenhizer, H., Salmon, V., Schädel, C., Strauss, J., Treat, C., and Turetsky, M.: Permafrost and Climate Change: Carbon Cycle Feedbacks From the Warming Arctic, Annu. Rev. Environ. Resour., 47, 343–371, https://doi.org/10.1146/annurev-environ-012220-011847, 2022.

Shaver, G. R. and Chapin, F. S.: Response to Fertilization by Various Plant Growth Forms in an Alaskan Tundra: Nutrient Accumulation and Growth, Ecology, 61, 662–675, https://doi.org/10.2307/1937432, 1980.

Sen, P. K. Estimates of the Regression Coefficient Based on Kendall's Tau. Journal of the American statistical Association, 63(324): 1379, doi:10.2307/2285891, 1968.

https://doi.org/10.5194/egusphere-2026-3328
Preprint. Discussion started: 3 July 2026

Smith, S. L., Romanovsky, V. E., Lewkowicz, A. G., Burn, C. R., Allard, M., Clow, G. D., Yoshikawa, K., and Throop, J.: Thermal state of permafrost in North America: a contribution to the international polar year, Permafr. Periglac. Process., 21, 117–135, https://doi.org/10.1002/ppp.690, 2010.

Swanson, D. K.: Permafrost thaw-related slope failures in Alaska's Arctic National Parks, *c* . 1980–2019, Permafr. Periglac. Process., 32, 392–406, https://doi.org/10.1002/ppp.2098, 2021.

Tieszen, L. L.: Photosynthesis in the Principal Barrow, Alaska, Species: A Summary of Field and Laboratory Responses, in: Vegetation and Production Ecology of an Alaskan Arctic Tundra, vol. 29, edited by: Tieszen, L. L., Springer New York, New York, NY, 241–268, https://doi.org/10.1007/978-1-4612-6307-4_10, 1978.

Torn, M. and Dengel, S.: AmeriFlux US-NGC NGEE Arctic Council, https://doi.org/10.17190/AMF/1634883, 2020.

Turetsky, M. R., Abbott, B. W., Jones, M. C., Anthony, K. W., Olefeldt, D., Schuur, E. A. G., Grosse, G., Kuhry, P., Hugelius, G., Koven, C., Lawrence, D. M., Gibson, C., Sannel, A. B. K., and McGuire, A. D.: Carbon release through abrupt permafrost thaw, Nat. Geosci., 13, 138–143, https://doi.org/10.1038/s41561-019-0526-0, 2020.

Vieira, G., Bockheim, J., Guglielmin, M., Balks, M., Abramov, A. A., Boelhouwers, J., Cannone, N., Ganzert, L., Gilichinsky, D. A., Goryachkin, S., López-Martínez, J., Meiklejohn, I., Raffi, R., Ramos, M., Schaefer, C., Serrano, E., Simas, F., Sletten, R., and Wagner, D.: Thermal state of permafrost and active-layer monitoring in the antarctic: Advances during the international polar year 2007–2009, Permafr. Periglac. Process., 21, 182–197, https://doi.org/10.1002/ppp.685, 2010.

Vogel, J., Schuur, E. A. G., Trucco, C., and Lee, H.: Response of CO_2 exchange in a tussock tundra ecosystem to permafrost thaw and thermokarst development, J. Geophys. Res. Biogeosciences, 114, 2008JG000901, https://doi.org/10.1029/2008JG000901, 2009.

Voigt, C., Lamprecht, R. E., Marushchak, M. E., Lind, S. E., Novakovskiy, A., Aurela, M., Martikainen, P. J., and Biasi, C.: Warming of subarctic tundra increases emissions of all three important greenhouse gases – carbon dioxide, methane, and nitrous oxide, Glob. Change Biol., 23, 3121–3138, https://doi.org/10.1111/gcb.13563, 2017.

Walker, D. A., Epstein, H. E., Romanovsky, V. E., Ping, C. L., Michaelson, G. J., Daanen, R. P., Shur, Y., Peterson, R. A., Krantz, W. B., Raynolds, M. K., Gould, W. A., Gonzalez, G., Nicolsky, D. J., Vonlanthen, C. M., Kade, A. N., Kuss, P., Kelley, A. M., Munger, C. A., Tarnocai, C. T., Matveyeva, N. V., and Daniëls, F. J. A.: Arctic patterned-ground ecosystems: A synthesis of field studies and models along a North American Arctic Transect, J. Geophys. Res. Biogeosciences, 113, 2007JG000504, https://doi.org/10.1029/2007JG000504, 2008.

Walter, K. M., Smith, L. C., and Stuart Chapin, F.: Methane bubbling from northern lakes: present and future contributions to the global methane budget, Philos. Trans. R. Soc. Math. Phys. Eng. Sci., 365, 1657–1676, https://doi.org/10.1098/rsta.2007.2036, 2007.

Wang, G., Peng, Y., Chen, L., Abbott, B. W., Ciais, P., Kang, L., Liu, Y., Li, Q., Peñuelas, J., Qin, S., Smith, P., Song, Y., Strauss, J., Wang, J., Wei, B., Yu, J., Zhang, D., and Yang, Y.: Enhanced response of soil respiration to experimental warming upon thermokarst formation, Nat. Geosci., 17, 532–538, https://doi.org/10.1038/s41561-024-01440-2, 2024.

Wang, T., Liu, D., Piao, S., Wang, Y., Wang, X., Guo, H., Lian, X., Burkhart, J. F., Ciais, P., Huang, M., Janssens, I., Li, Y., Liu, Y., Peñuelas, J., Peng, S., Yang, H., Yao, Y., Yin, Y., and Zhao, Y.: Emerging negative impact of warming on summer carbon uptake in northern ecosystems, Nat. Commun., 9, 5391, https://doi.org/10.1038/s41467-018-07813-7, 2018.

Ward Jones, M. K., Pollard, W. H., and Jones, B. M.: Rapid initialization of retrogressive thaw slumps in the Canadian high Arctic and their response to climate and terrain factors, Environ. Res. Lett., 14, 055006, https://doi.org/10.1088/1748-9326/ab12fd, 2019.

https://doi.org/10.5194/egusphere-2026-3328
Preprint. Discussion started: 3 July 2026

1011 Webb, E. E., Schuur, E. A. G., Natali, S. M., Oken, K. L., Bracho, R., Krapek, J. P., Risk, D., and Nickerson, N. R.:
1012 Increased wintertime CO_2 loss as a result of sustained tundra warming, J. Geophys. Res. Biogeosciences, 121, 249–
1013 265, https://doi.org/10.1002/2014JG002795, 2016.

1014 Webb, H., Fuchs, M., Abbott, B. W., Douglas, T. A., Elder, C. D., Ernakovich, J. G., Euskirchen, E. S., Göckede, M.,
1015 Grosse, G., Hugelius, G., Jones, M. C., Koven, C., Kropp, H., Lathrop, E., Li, W., Loranty, M. M., Natali, S. M.,
1016 Olefeldt, D., Schädel, C., Schuur, E. A. G., Sonnentag, O., Strauss, J., Virkkala, A.-M., and Turetsky, M. R.: A Review
1017 of Abrupt Permafrost Thaw: Definitions, Usage, and a Proposed Conceptual Framework, Curr. Clim. Change Rep.,
1018 11, 7, https://doi.org/10.1007/s40641-025-00204-3, 2025.

1019 World Weather Online: Council Annual Weather Averages [online] Available from:
1020 https://www.worldweatheronline.com/council-weather-averages/alaska/us.aspx. (Accessed April 2026), 2026.
1021 Zoomash Ltd, 3rd Floor, 86-90 Paul Street, London, Hackney, EC2A 4NE, UK.
1022
1023 Wutzler, T., Lucas-Moffat, A., Migliavacca, M., Knauer, J., Sickel, K., Sigut, Menzer, O. & Reichstein, M. Basic and
1024 extensible post-processing of eddy covariance flux data with REddyProc. Biogeosciences, Copernicus, 15, doi:
1025 10.5194/bg-15-5015-2018, 2018
1026
1027 Xu, L., Furtaw, M. D., Madsen, R. A., Garcia, R. L., Anderson, D. J., and McDermitt, D. K.: On maintaining pressure
1028 equilibrium between a soil CO_2 flux chamber and the ambient air, J. Geophys. Res. Atmospheres, 111, 2005JD006435,
1029 https://doi.org/10.1029/2005JD006435, 2006.

1030 Zhao, L., Wu, Q., Marchenko, S. S., and Sharkhuu, N.: Thermal state of permafrost and active layer in Central Asia
1031 during the international polar year, Permafr. Periglac. Process., 21, 198–207, https://doi.org/10.1002/ppp.688, 2010.

1032 Zona, D., Lipson, D. A., Zulueta, R. C., Oberbauer, S. F., and Oechel, W. C.: Microtopographic controls on ecosystem
1033 functioning in the Arctic Coastal Plain, J. Geophys. Res., 116, G00I08, https://doi.org/10.1029/2009JG001241, 2011.

1034 Zona, D., Gioli, B., Commane, R., Lindaas, J., Wofsy, S. C., Miller, C. E., Dinardo, S. J., Dengel, S., Sweeney, C.,
1035 Karion, A., Chang, R. Y.-W., Henderson, J. M., Murphy, P. C., Goodrich, J. P., Moreaux, V., Liljedahl, A., Watts, J.
1036 D., Kimball, J. S., Lipson, D. A., and Oechel, W. C.: Cold season emissions dominate the Arctic tundra methane
1037 budget, Proc. Natl. Acad. Sci., 113, 40–45, https://doi.org/10.1073/pnas.1516017113, 2016.

1038 Zona, D., Lafleur, P. M., Hufkens, K., Gioli, B., Bailey, B., Burba, G., Euskirchen, E. S., Watts, J. D., Arndt, K. A.,
1039 Farina, M., Kimball, J. S., Heimann, M., Göckede, M., Pallandt, M., Christensen, T. R., Mastepanov, M., López-
1040 Blanco, E., Dolman, A. J., Commane, R., Miller, C. E., Hashemi, J., Kutzbach, L., Holl, D., Boike, J., Wille, C., Sachs,
1041 T., Kalhori, A., Humphreys, E. R., Sonnentag, O., Meyer, G., Gosselin, G. H., Marsh, P., and Oechel, W. C.: PAN-
1042 ARCTIC soil moisture control on tundra carbon sequestration and plant productivity, Glob. Change Biol., 29, 1267–
1043 1281, https://doi.org/10.1111/gcb.16487, 2023.